(12) LEVEL II

NWC TP 6049

Convective Burning in Isolated Solid Propellant Cracks

by
K. K. Kuo
R. L. Kovalcin
S. J. Ackman
Pennsylvania State University
for the
Research Department

FEBRUARY 1979

Naval Weapons Center
CHINA LAKE, CALIFORNIA 93555

Naval Weapons Center

AN ACTIVITY OF THE NAVAL MATERIAL COMMAND

FOREWORD

This report summarizes progress made in the study of convective burning in solid propellant cracks. The study was performed by Pennsylvania State University under Contract No. N60530-77-C-0078 during the period 1 February 1977 through 31 January 1978. The contract was monitored by the Naval Weapons Center and funded by the Naval Surface Weapons Center under Task B0003001.

This report has been reviewed for technical accuracy by Harold H. Bradley, Jr.

Because of the continuing nature of this research, refinements and modifications may be made in the future.

Approved by
E. B. ROYCE, *Head*
Research Department
15 January 1979

Under authority of
W. L. HARRIS
RAdm., U.S. Navy
Commander

Released for publication by
R. M. HILLYER
Technical Director

NWC Technical Publication 6049

Published by . . . . . Technical Information Department
Collation . . . . . Cover, 34 leaves
First printing . . . . . 260 unnumbered copies

UNCLASSIFIED

SECURITY CLASSIFICATION OF THIS PAGE *(When Data Entered)*

(18) (19) **REPORT DOCUMENTATION PAGE**

READ INSTRUCTIONS BEFORE COMPLETING FORM

1. REPORT NUMBER: NWC TP-6049
2. GOVT ACCESSION NO.
3. RECIPIENT'S CATALOG NUMBER (9)
4. TITLE (and Subtitle) (6): CONVECTIVE BURNING IN ISOLATED SOLID PROPELLANT CRACKS
5. TYPE OF REPORT & PERIOD COVERED: Research Progress Report, 1 Feb 1977 – 31 Jan 1978
6. PERFORMING ORG. REPORT NUMBER
7. AUTHOR(s) (10): K. K. Kuo, R. L. Kovalcin, S. J. Ackman
8. CONTRACT OR GRANT NUMBER(s) (15): N60530-77-C-0078
9. PERFORMING ORGANIZATION NAME AND ADDRESS: Pennsylvania State University, University Park, Pennsylvania 16802
10. PROGRAM ELEMENT, PROJECT, TASK AREA & WORK UNIT NUMBERS: Task B0003001
11. CONTROLLING OFFICE NAME AND ADDRESS: Naval Weapons Center, China Lake, California 93555
12. REPORT DATE (11): February 1979
13. NUMBER OF PAGES: 66
14. MONITORING AGENCY NAME & ADDRESS *(if different from Controlling Office)* (12) 66p.
15. SECURITY CLASS. *(of this report)*: UNCLASSIFIED
15a. DECLASSIFICATION/DOWNGRADING SCHEDULE
16. DISTRIBUTION STATEMENT *(of this Report)*: Approved for public release; distribution unlimited.

17. DISTRIBUTION STATEMENT *(of the abstract entered in Block 20, if different from Report)*
18. SUPPLEMENTARY NOTES
19. KEY WORDS *(Continue on reverse side if necessary and identify by block number)*

Controlling parameters in convective burning	Flame propagation chamber
Convective burning	Propellant crack combustion
Crack tip ignition	Propellant sample preparation
Deflagration-to-detonation transition	Transient ignition phenomena
	Windowed crack combustion

20. ABSTRACT *(Continue on reverse side if necessary and identify by block number)*

(See back of form)

DD FORM 1 JAN 73 1473 EDITION OF 1 NOV 65 IS OBSOLETE S/N 0102-014-6601

UNCLASSIFIED

SECURITY CLASSIFICATION OF THIS PAGE *(When Data Entered)*

278 650

(U) *Convective Burning in Isolated Solid Propellant Cracks*, by K. K. Kuo, R. L. Kovalcin, and S. J. Ackman, Pennsylvania State University. China Lake, Calif., Naval Weapons Center, February 1979. 66 pp. (NWC TP 6049, publication UNCLASSIFIED.)

(U) The theoretical model for describing flame spreading and combustion phenomena inside an isolated solid propellant crack has been modified: (1) to solve for the subsurface temperature profile in facilitating the study of dynamic burning effect on crack cavity pressurization, (2) to incorporate the "Dipstick" ignition criterion postulated by C. F. Price of the Naval Weapons Center, and (3) to improve the numerical treatment of the gas-dynamic boundary conditions at the opening of the propellant crack. In addition, the governing equations are nondimensionalized and a number of dimensionless parameters have been obtained.

(U) Experimentally, after numerous attempts, a reproducible solid propellant ignition system has been developed and tested to produce high pressurization rates and short ignition delays so that the flame spreading and the overall transient convective burning process can be recorded on high-speed motion pictures with adequate time resolutions. A number of test firings were conducted with crack specimens of various dimensions and igniter strengths. It is found that the strength of the igniter is extremely influential to the rate of flame spreading and crack combustion. The gap width of the crack is also found to be important in producing significant pressure gradients along the crack, especially during the flame spreading interval.

(U) The comparison of the theoretical results with experimental data showed good qualitative agreement. Although the quantitative comparison showed a reasonable match, some differences were noted and discussed. In order to improve the quantitative prediction of the experimental results, the solid–phase mechanical deformation must be incorporated with the combustion code. Areas for technological gaps in the crack combustion studies are also identified for future investigations.

CONTENTS

INTRODUCTION

Achieving high specific impulses by increasing the solids loading of highly energetic materials (e.g., HMX) in solid propellants has been an objective of the rocket industry for many years. At a very high solids loading there is an increased probability that cracks or flaws can develop in the propellant grain. These defects may originate in solid propellants as a result of (1) improper manufacturing processes so that bubbles and cavities are present in the propellant, (2) the aging effect during storage, (3) nonuniform stress loading associated with large pressure gradient during propellant ignition process, (4) the impairment of the adhesive bond between the fuel and oxidizer due to mechanical stresses during combustion, (5) the formation of micropores due to thermal stresses, and (6) the damage of propellant charges during transportation.

On a microscopic level it is believed that cracks occur in heterogeneous or composite propellants due to an adhesive failure between the rubbery binder and the high solids loading (up to approximately 90% on a volume basis) of oxidizer particles and other granular fuel additives. Once the adhesion between these particles has failed, microscopic vacuoles form near the particles and readily propagate to become finite cracks. In general, these finite cracks can degrade the mechanical properties and structural integrity of solid propellant grains.

The extent to which crack combustion can reduce the reliability of solid rocket motors has been one of the main concerns in the development of high-energy propellants. The cracks can allow the hot gases to penetrate the cavity and can provide additional surface area for ignition and combustion. The combustion processes inside a propellant crack can produce shock-like compression waves and may also lead to a pressure build-up which could cause mechanical deformation, crack propagation, and possible deflagration-to-detonation transition (DDT). Even if, under certain conditions, the convective burning does not lead to catastrophic failure, the combustion inside the propellant crack can cause the performance of a rocket motor to deviate significantly from expectations.

Although imperfections in solid propellant grains may be distributed in an irregular intricate network, a rational starting-point for understanding the phenomena involved in crack combustion is to consider a simple ordered system--a single isolated crack. For such a system it is desirable to establish a criterion for stable combustion without catastrophic crack propagation or incipient detonation; the delineation of a

safe domain of governing parameters is the ultimate goal. But before it can be achieved, a realistic theoretical model describing both the mechanical deformation and transient combustion processes inside a propellant crack has to be established and experimentally verified.

The primary objectives of the research effort were as follows:

1. To conduct experimental firings with single-pore propellant grains for verification of the theoretical model and for establishment of a fundamental data base in crack combustion.

2. To modify the theoretical model and computer program for obtaining the in-depth thermal profile of the propellant so that the dynamic burning behavior can be studied.

3. To consider various ignition criterions such as the "Dipstick" criterion; the critical surface temperature criterion; or the two-temperature, surface-ignition criterion for the calculation of flame spreading rates.

4. To nondimensionalize the gas-dynamic and heat-transfer equations in order to obtain a set of dimensionless parameters that characterize crack combustion.

5. To study the compatibility of the crack combustion program with a nonlinear stress analysis program so that the stress field near the crack tip can be evaluated for determination of crack propagation due to pressure loading. Also, to select a well-developed structural analysis program suitable for coupling with the crack combustion code.

BACKGROUND

During previous research investigations conducted at the Pennsylvania State University, substantial progress was achieved in the study of the convective burning processes inside a solid propellant crack.[1-3] Some of the important theoretical and experimental achievements are given as follows:

---

[1]Naval Weapons Center. *Transient Combustion in Solid Propellant Cracks*, by K. K. Kuo, et al., Pennsylvania State University. China Lake, CA, NWC, October 1977. (NWC TP 5943, publication UNCLASSIFIED.)

[2]K. K. Kuo, A. T. Chen, and T. R. Davis. "Transient Flame Spreading and Combustion Processes Inside a Solid Propellant Crack," presented at AIAA 15th Aerospace Sciences Meeting, Los Angeles, CA, January 1977. (AIAA Preprint No. 77-14.)

[3]K. K. Kuo and D. R. McClure. "Transient Combustion Processes in Solid Propellant Cracks," Semi-Annual Report to the Aerothermochemistry Division of the Naval Weapons Center, August 1977. (Report UNCLASSIFIED.)

1. An extensive literature survey of theoretical and experimental investigations on flame propagation in cracks has been conducted. A survey of heat-transfer and flow-resistance empirical correlations on flow through chemically inert cracks was performed.

2. A quasi-one-dimensional theoretical model has been developed to describe the transient combustion phenomena in a propellant crack. The theoretical model can be used to predict the wave phenomena, heat-transfer processes from gas to propellant surface flame propagation, and resultant pressurization at various locations along the propellant cavity.

3. A computer program has been developed based on the above theoretical model to predict the flame-spreading and combustion phenomena inside a crack. The program can be utilized to conduct parametric studies on the effects of crack gap width, depth, cross-sectional area distribution, propellant burning rate, ignition (runaway) temperature, and other physiochemical properties of the propellant.

4. A laboratory-sized solid-propellant combustion chamber, utilizing current state-of-the-art techniques in high-speed photography and transient pressure recording, has been developed to obtain data for verification of the theoretical model. The facility permits the simultaneous acquisition of the time-correlated flame-spreading rate and pressure wave propagation.

THEORETICAL WORK

NONDIMENSIONALIZATION OF THE GAS-DYNAMIC AND HEAT-TRANSFER EQUATIONS GOVERNING THE CONVECTIVE BURNING PROCESSES IN CRACKS

The Russian work[4,5] suggests that the transition from conductive (normal layer-to-layer) burning to convective (gas-penetration) burning for gas-permeable propellants occurs when the Andreev number, An, is above a critical value. The Andreev number is defined as

---

[4]A. F. Belyaev, et al. "Development of Burning in a Single Pore," in *Transition of Combustion of Condensed Systems to Detonation*. Science Publisher, Moscow, 1973. Chapter 3, Part B and Chapter 5, Part A.

[5]A. D. Margolin and S. V. Chuiko. "Combustion Instability of a Porous Charge with Spontaneous Penetration of the Combustion Products into the Pores," *Combustion, Explosion and Shock Waves*. Vol. 2, No. 3, 1966.

$$An = \frac{\rho_c r_b C_{pr} d_p}{\lambda_{pr}} \qquad (1)$$

where

ρ_c = density of the gas-permeable (porous) charge
r_b = burning rate
C_{pr} = specific heat of the condensed phase
d_p = diameter of the pore
λ_{pr} = thermal conductivity of the propellant

The Andreev number is similar to the Peclet number in its physical meaning; it represents the ratio of convective heat flux to conductive heat flux. This finding is helpful in defining the boundary beyond which there is spontaneous penetration of the combustion products into the pores.

Once the gas has penetrated into the pores of a gas-permeable propellant, the Andreev number no longer governs the flame spreading and combustion phenomena inside the pore. Several questions can be raised immediately in regard to the governing dimensionless parameters which dominate the physical processes in propellant crack combustion. First, what are the dimensionless parameters which are important to consider in the convective burning stage of the multifaceted problem of DDT? Second, is the Andreev number the only parameter in governing the gas penetration condition into cracks? Would the rate of gas pressurization at the crack opening also be important in determining the state of gas penetration at the crack entrance? Third, would the Andreev number be a natural dimensionless group obtained from the governing equations? If not, can it be constructed from other dimensionless parameters obtained from the nondimensionalization procedure?

To answer these questions and also to determine the controlling dimensionless parameters that characterize the convective burning problem, it is worthwhile to nondimensionalize the governing gas-dynamic and heat transfer equations. It should be noted that the complete groups of governing parameters cannot be obtained without looking at the coupled solid mechanics equations for the solid propellant. However, for the time being, it is useful to obtain a set of dimensionless parameters from the crack combustion model before coupling it to solid mechanics; the controlling parameters may suggest a systematic way of performing laboratory tests and logical ways of correlating experimental data. Therefore, the following nondimensionalization procedures are carried out.

To simplify the nondimensionalization procedure, the terms of secondary importance in the gas-dynamic equations were neglected. After neglecting the body force term and the normal viscous stress gradient

term in the momentum equation and the terms representing the gas-phase heat conduction, body force work and the normal viscous stress work from the energy equation, the gas dynamic equations in the quasi-one-dimensional crack combustion model become

$$\frac{\partial(\rho A_p)}{\partial t} + \frac{\partial(\rho A_p u)}{\partial x} = r_b \rho_{pr} p_b \tag{2}$$

$$\frac{\partial(\rho A_p u)}{\partial t} + \frac{\partial(\rho A_p u^2)}{\partial x} = -g\, A_p \frac{\partial P}{\partial x} - p_w \tau_w g \cos\theta_w$$

$$- (\rho_{pr} r_b p_b)\, V_{gf} \sin\theta_w \tag{3}$$

$$\frac{\partial(\rho A_p E)}{\partial t} + \frac{\partial(\rho A_p E u)}{\partial x} = \rho_{pr} r_b p_b h_f - \frac{1}{J}\frac{\partial}{\partial x}(A_p P u)$$

$$-\bar{h}_{c_p} p_b (T - T_{ps}) - \bar{h}_{c_w} (p_w - p_b)(T - T_{ws}) \tag{4}$$

The propellant surface temperature variation equation is used in the nondimensionalization to replace the transient heat-conduction equation and its initial and boundary conditions; thus, we have at a given axial location

$$\frac{d\,T_{ps}}{dt} = \frac{4\alpha_{pr} \bar{h}_{c_p}^{\,2} (T - T_{ps})^3}{3\,\lambda_{pr}^{\,2} (T_{ps} - T_{pi})(2T - T_{ps} - T_{pi})} \tag{5}$$

The dimensionless parameters are defined as follows:

$$\tilde{x} \equiv \frac{x}{x^*} = \frac{x}{L}, \quad \tilde{t} \equiv \frac{t}{t^*} \tag{6}$$

$$\tilde{P} \equiv \frac{P}{P^*}, \quad \tilde{u} \equiv \frac{u}{u^*}, \quad \tilde{\rho} \equiv \frac{\rho}{\rho^*} \tag{7}$$

$$\tilde{T} \equiv \frac{T - T_i}{T_f - T_i} \equiv \frac{T - T_i}{T^*}, \quad \tilde{E} = \frac{E}{E^*} \tag{8}$$

$$\tilde{T}_{ps} \equiv \frac{T_{ps} - T_i}{T_{ign} - T_i} \equiv \frac{T_{ps} - T_i}{T_{ign}^*},$$

$$\tilde{T}_{ws} \equiv \frac{T_{ws} - T_i}{T_{ign} - T_i} \equiv \frac{T_{ws} - T_i}{T_{ign}^*} \tag{9}$$

$$\tilde{A}_p \equiv \frac{A_p}{A_{p_i}}, \quad \tilde{A}_b \equiv \frac{A_b}{A_{b_i}} \tag{10}$$

$$\tilde{p}_w \equiv \frac{p_w}{p_{w_i}}, \quad \tilde{p}_b \equiv \frac{p_b}{p_{b_i}} \tag{11}$$

$$\tilde{r}_b = \frac{r_b}{r_b^*}, \quad \tilde{\tau}_w = \frac{\tau_w}{\tau_w^*}, \quad \tilde{h}_f = \frac{h_f}{C_p T^*} \tag{12}$$

and

$$\tilde{h}_{c_p} = \frac{\bar{h}_{c_p}}{h_c^*}, \quad \tilde{h}_{c_w} = \frac{\bar{h}_{c_w}}{h_c^*} \tag{13}$$

Some of the reference parameters, designated with superscript *, can be selected readily without any difficulty. For example, the characteristic length along the crack should be the length of the crack, L, i.e.,

$$x^* = L \tag{14}$$

The reference port area can be taken to be the initial average port area

$$A_{p_i} \equiv \frac{D_{H_i} p_{w_i}}{4} \tag{15}$$

where D_{H_i} represents the initial hydraulic diameter of the pore. The reference burning area can be selected to be

$$A_{b_i} = L p_{b_i} \tag{16}$$

Naturally, the initial average wetted perimeter p_{w_i} and the initial average burning perimeter p_{b_i} should be used as reference quantities shown in Eq. (11).

Based upon the definition given in Eq. (8), the reference temperature for the gas temperature is selected to be

$$T^* \equiv T_f - T_i \tag{17}$$

The reference gas density can be defined by the perfect gas law as

$$\rho^* = \frac{P^*}{RT^*} \tag{18}$$

where P^*, the reference pressure, must be properly selected; and the value of P^* can be used to determine the burning rate, r_b^* as

$$r_b^* = a(P^*)^n \tag{19}$$

After balancing the mass burning rate with the mass flow rate out of a crack at the choked condition, P^* can be selected as

$$P^* = \left[\frac{a}{\Gamma(\gamma)}\left(\frac{A_{b_i}}{A_{p_i}}\right)\rho_{pr}\sqrt{\frac{RT_f}{g}}\right]^{\frac{1}{1-n}} \tag{20}$$

where

$$\Gamma(\gamma) \equiv \sqrt{\gamma\left(\frac{2}{\gamma+1}\right)^{\frac{\gamma+1}{\gamma-1}}} \tag{21}$$

The most difficult reference parameter to select in the nondimensionalization is the appropriate t*. There are many characteristic times one can consider in the crack combustion study. To name a few, we have: flow residence time, flame propagation time, ignition delay time, thermal wave relaxation time in solid propellant (time associated with thermal wave propagation during propellant regression), pressure wave traveling time from crack entrance to tip, characteristic time related to the initial pressurization rate at the crack entrance, the time to reach maximum pressure in the overall transient event, etc. These times are not of the same order of magnitude. Also, these reference times are associated with different length scales and velocities. There are many length scales that can be enumerated. For example, crack length, gap width, hydraulic diameter, crack surface roughness, flame stand-off distance, thermal wave penetration depth due to convective heating, heated layer thickness of the burning propellant, etc.

After a detailed consideration, the ignition delay time, which is closely related to the flame spreading time, is taken to be the most important time scale in convective burning. By setting $T_{pi}^{\sim} = T_i$ and nondimensionalizing Eq. (5) according to the definitions given in Eq. (6), (8), (9), and (13), we have

$$\frac{d\tilde{T}_{ps}}{d\tilde{t}} = \frac{4\tilde{h}_c\left[\tilde{T} - \left(\frac{T_{ign} - T_i}{T_f - T_i}\right)\tilde{T}_{ps}\right]^3}{3\tilde{T}_{ps}\left[2\tilde{T} - \left(\frac{T_{ign} - T_i}{T_f - T_i}\right)\tilde{T}_{ps}\right]} \tag{22}$$

if we define

$$t^* \equiv \frac{\lambda_{pr}^2}{\alpha_{pr} h_c^{*2}}\left(\frac{T_{ign} - T_i}{T_f - T_i}\right)^2 \tag{23}$$

where h_c^*, the reference heat-transfer coefficient, must be defined. Before the explicit form of h_c^* is defined, it is interesting to see the physical meaning of the following parameter formed from Eq. (23)

$$\frac{t^* \alpha_{pr} h_c^{*2}}{\lambda_{pr}^2} \sim \left(\frac{\delta_{th} h_c^*}{\lambda_{pr}}\right)^2 = (Bi^*)^2 \tag{24}$$

where Bi^*, the Biot modulus, represents the ratio of internal thermal resistance of the propellant to the external thermal resistance of the convective boundary at the gas-propellant interface.

Based upon the Reynolds analogy for turbulent flow in a tube and the well-established Blasius flow-resistance formula, h_c^* can be related to u^* according to

$$h_c^* = 0.0038\, C_p \rho^* u^* \tag{25}$$

The characteristic velocity, u^*, can be related to t^* by

$$u^* = \frac{L}{t^*} = \frac{\lambda_{pr}^2}{0.1444 \times 10^{-4}\, L \alpha_{pr} C_p^2 \rho^{*2}}\left(\frac{T_{ign} - T_i}{T_f - T_i}\right)^2 \tag{26}$$

The advantage of using the above relationship between u^* and t^* is to have both the time-variation and the space-variation of the mass, momentum and energy in the governing equations in the same order or magnitude.

In addition to the preceding reference parameters, we further define

$$\mu^* = 8.699 \times 10^{-7} \times (M_w)^{0.5} \, (T^*)^{0.65} \tag{27}$$

based upon Svehla's formula.[6] The reference wall shear stress on crack surfaces can be defined by using the Weisbach friction coefficient, f, as

$$\tau_w^* = \frac{f}{8g} \rho^* u^{*2} \tag{28}$$

Also, we define

$$E^* = C_p T^* \quad \text{and} \quad M^* \equiv \frac{u^{*2}}{\gamma g R T^*} \tag{29}$$

After nondimensionalization, the governing gas-dynamic equations (2)-(4) become

$$\frac{\partial(\tilde{\rho}\tilde{A}_p)}{\partial \tilde{t}} + \frac{\partial(\tilde{\rho}\tilde{A}_p\tilde{u})}{\partial \tilde{x}} = \left(\frac{A_{b_i}}{A_{p_i}}\right)\left(\frac{\rho_{pr} r_b^*}{\rho^* u^*}\right) \tilde{r}_b \tilde{p}_b \tag{30}$$

$$\frac{\partial(\tilde{\rho}\tilde{A}_p\tilde{u})}{\partial \tilde{t}} + \frac{\partial(\tilde{\rho}\tilde{A}_p\tilde{u}^2)}{\partial \tilde{x}} = -\frac{\tilde{A}_p}{\gamma M^{*2}} \frac{\partial \tilde{P}}{\partial \tilde{x}} - \left(\frac{f}{8}\right)\left(\frac{A_{w_i}}{A_{p_i}}\right) \tilde{\tau}_w \tilde{p}_w \cos\theta_w$$

$$- \left(\frac{A_{b_i}}{A_{p_i}}\right)\left(\frac{\rho_{pr} r_b^*}{\rho^* u^*}\right)^2 \tilde{r}_b^2 \tilde{p}_b \frac{\sin\theta_w}{\tilde{\rho}} \tag{31}$$

---

[6]National Aeronautics and Space Administration. *Estimated Viscosities and Thermal Conductivities of Gases at High Temperatures*, by R. A. Svehla. Lewis Research Center, Cleveland, OH, NASA, 1962. (NASA TR R-132, publication UNCLASSIFIED.)

$$\frac{\partial(\tilde{\rho}\tilde{A}_p\tilde{E})}{\partial\tilde{t}} + \frac{\partial(\tilde{\rho}\tilde{A}_p\tilde{E}\tilde{u})}{\partial\tilde{x}} = \left(\frac{A_{b_i}}{A_{p_i}}\right)\left(\frac{\rho_{pr}r_b^*}{\rho^* u^*}\right)\tilde{r}\,\tilde{p}_b\tilde{h}_f - \frac{\gamma-1}{\gamma}\frac{\partial}{\partial\tilde{x}}(\tilde{A}_p\tilde{P}\tilde{u})$$

$$- \left(\frac{A_{b_i}}{A_{p_i}}\right)\left(\frac{h_c^*}{\rho^* u^* C_p}\right)\tilde{h}_{cp}\tilde{p}_b\left[\tilde{T} - \left(\frac{T_{ign} - T_i}{T_f - T_i}\right)\tilde{T}_{ps}\right]$$

$$- \left(\frac{A_{w_i}}{A_{p_i}}\tilde{p}_w - \frac{A_{b_i}}{A_{p_i}}\tilde{p}_b\right)\left(\frac{h_c^*}{\rho^* u^* C_p}\right)\tilde{h}_{c_w}\left[\tilde{T} - \left(\frac{T_{ign} - T_i}{T_f - T_i}\right)\tilde{T}_{ws}\right] \quad (32)$$

The dimensionless parameters shown in the governing equations (30)-(32) and (22) are [through the use of Eq. (23) and (24)]:

$$\frac{\rho_{pr}r_b^*}{\rho^* u^*}, \quad \frac{A_{b_i}}{A_{p_i}}, \quad \frac{A_{w_i}}{A_{p_i}}, \quad f, \quad M^*, \quad \frac{h_c^*}{\rho^* u^* C_p},$$

$$\frac{T_{ign} - T_i}{T_f - T_i}, \quad Bi^*$$

The first group can be defined as the mass blowing parameter, B_m^*

$$B_m^* \equiv \frac{\rho_{pr}r_b^*}{\rho^* u^*} = \frac{\text{mass burning rate per unit burning area}}{\text{mass flow rate per unit port area}} \quad (33)$$

The second group can be expressed as

$$\frac{A_{b_i}}{A_{p_i}} = 4\left(\frac{L}{D_{H_i}}\right)\left(\frac{p_{b_i}}{p_{w_i}}\right) \quad (34)$$

When the burning perimeter is equal to the wetted perimeter, the area ratio is directly related to the length-to-hydraulic diameter ratio of the crack. The third group can be replaced by $4(L/D_{H_i})$.

The friction coefficient for turbulent flow inside a crack of a given surface roughness and condition of gasification can be expressed in the following functional form

$$f = f\left(Re^*_{D_{H_i}}, \frac{\varepsilon}{D_{H_i}}, B_m^*\right) \tag{35}$$

where the Reynolds number, $Re^*_{D_{H_i}}$, can be defined by

$$Re^*_{D_{H_i}} \equiv \frac{\rho^* u^* D_{H_i}}{\mu^*} \tag{36}$$

and ε/D_{H_i} represents the ratio of surface roughness to the hydraulic diameter of the crack. The ratio of h_c^* to $\rho^* u^* C_p$ can be defined as the Stanton number, St^*, i.e.

$$St^* \equiv \frac{h_c^*}{\rho^* u^* C_p} \tag{37}$$

Other dimensionless parameters which should be considered are:

$$\frac{\alpha_{pr}}{r_b^{*2} P_c}\left(\frac{dP_c}{dt}\right)_i, \quad \frac{\delta_{fs}}{\delta_{gap}}, \quad \frac{u_{fp}}{u^*}.$$

Among these parameters, the first group comes from the boundary conditions at the crack entrance; it represents the ratio of the thermal wave relaxation time for burning propellant to the time characterizing the initial pressurization at the crack entrance. The second group represents the ratio of the flame stand-off distance to the crack gap width; it is important in the consideration of incomplete combustion due to an extremely small gap width between the two opposite crack surfaces. The last group represents the ratio of the unknown flame-propagation rate to the characteristic velocity u^* defined in Eq. (26).

Finally, these dimensionless parameters can be put into the following functional form

$$\frac{u_{fp}}{u^*} = \frac{u_{fp}}{u^*}\left[\frac{\alpha_{pr}}{r_b^{*2} P_c}\left(\frac{dP_c}{dt}\right)_i, \frac{\delta_{fs}}{\delta_{gap}}, Bi^*, B_m^*, \frac{p_{b_i}}{p_{w_i}}, \frac{L}{D_{H_i}}, \frac{\varepsilon}{D_{H_i}}, Re^*_{D_{H_i}}, M^*, St^*, \frac{T_{ign}-T_i}{T_f-T_i}\right] \tag{38}$$

It should be noted that these parameters do not include the effect of mechanical deformation and damage. In our continuing research effort on crack combustion, the governing parameters associated with solid mechanics will be studied and incorporated into the dimensionless group.

SOLUTION OF THE SUBSURFACE TEMPERATURE DISTRIBUTION FROM TRANSIENT HEAT-CONDUCTION EQUATION

There are two major reasons for solving the transient heat-conduction equation. One reason is to incorporate the ignition criterion, such as the "Dipstick" ignition criterion, which requires the information of subsurface temperature profile. The other reason is to facilitate future investigation of the dynamic burning effect in propellant crack combustion. Recall that previously the propellant surface temperature at various stations along the crack wall was determined by Goodman's integral method[7] described in footnote 1. Currently, in order to obtain the information about the in-depth thermal response of the propellant, the transient heat conduction equation

$$\frac{\partial T_{pr}(y,t)}{\partial t} = \alpha_{pr} \frac{\partial^2 T_{pr}(y,t)}{\partial y^2} \tag{39}$$

with the following initial and boundary conditions

$$T_{pr}(y,0) = T_{pi} \tag{40}$$

$$T_{pr}(\infty,t) = T_{pi} \tag{41}$$

$$\frac{\partial T_{pr}(0,t)}{\partial y} = -\frac{\bar{h}_c(t)}{\lambda_{pr}} [T_{gas}(t) - T_{pr}(0,t)] \tag{42}$$

has been coded in a new subroutine for solution by an explicit, variable-mesh, finite-difference method. Equation (39) is used to obtain the propellant temperature distributions prior to ignition. The finite-difference and Goodman integral methods have been compared to an exact solution[8] of the heat flow in a semi-infinite solid with constant $\bar{h}_c$. Both approximate methods were found to be quite accurate (<3%). The in-depth temperature profiles will be used in future calculations to evaluate the effects of dynamic burning and the importance of thermal stresses in the finite element work.

---

[7]T. R. Goodman. "The Heating of Slabs with Arbitrary Heat Input," *Journal of the Aerospace Sciences*, Vol. 26, March 1959, pp. 183-188.

[8]P. J. Schneider. *Conduction Heat Transfer*. Addison-Wesley Publishing Company, Reading, Mass., 1955.

The "Dipstick" ignition criterion, postulated by Price,* has been incorporated in the crack combustion program. The concept of a critical gasification temperature and ignition temperature was added to this criterion to provide easier interfacing with the previous two-temperature, surface-ignition criterion ($T_{pr_{cri}} \simeq T_{pr_{ign}} = 460°K$ at $\delta_{ign} = 60$ μm) which revealed that the propellant surface temperature near the crack entrance may exceed 1000-1300°K before the substrate temperature at δ_{ign} reaches the ignition temperature. However, the onset of ignition can be established earlier by lowering $T_{pr_{cri}}$ or reducing δ_{ign}.

To have the maximum flexibility, the previously developed subroutine which uses the integral solution for the propellant surface temperature calculation, is retained in the computer program as an optional method in the computation of the flame spreading rate.

IMPROVEMENTS IN THE NUMERICAL TREATMENT OF GAS-PHASE BOUNDARY CONDITION

As pointed out by Price,* some steps in the numerical treatment of the gas-dynamic boundary condition for inflow could be improved. This deficiency has been rectified, and the program can now more accurately describe the influence of rapidly varying rocket chamber pressurizations on the subsonic and sonic inflow of gases. Some details of these changes are discussed below.

In the numerical computation of the gas dynamic boundary condition for the case of inflow into the crack, it was found that a quasi-steady approximation can be used to treat the flow from the rocket chamber into the crack entrance region. As long as the boundary station for partial differential equation solution is taken to be very close to the actual crack opening station ($\Delta L \leq 0.01$ cm), the pressure and gas temperature at the boundary station can be accurately determined from the isentropic relations of the actual or simulated rocket chamber conditions. The gas velocity at the boundary station is determined from an integration of the particle pathline in the Left Boundary Condition Subroutine (LBC). When the pressure at the boundary station is greater than the critical pressure required for choked flow, the gas velocity from the previous iteration and the new values of external stagnation pressure and temperature are used in a subsonic, isentropic relation to evaluate the new pressure and temperature at the boundary station. It is found that this technique works very well even for a rapidly varying rocket chamber pressure.

---

*Private communication with Channon F. Price, Naval Weapons Center, April 1977.

STUDY OF STRUCTURAL ANALYSIS PROGRAM

A literature survey on crack fracture and deformation has been conducted. The review of various well-developed finite element analysis programs has also been carried out. Of the numerous structural analysis codes (e.g., NONSAP, NASTRAN, TEXGAP), the modified version of NONSAP (NFAP) is considered to be the most suitable one to couple with the crack combustion code for the reasons discussed below.[9-11]

The modified version of NONSAP (NFAP) has been obtained from the University of Akron, Akron, Ohio and loaded on the PSU computer. The user's manual has been reviewed to determine the best way to streamline and couple the program with the combustion code. The important features of NFAP which are relevant to the research work on crack combustion are:

1. The program is an efficient, easily modifiable general stress analysis program with restart capabilities.

2. It can treat transient loading and inertia effects in two- and three-dimensional structures.

3. The code can treat geometric nonlinearities caused by large deformations.

4. NFAP also can treat material nonlinearities. It contains a special dummy overlay in which the user can supply, in a consistent manner, one's own form of the propellant constitutive equation.

EXPERIMENTAL SET-UP OF THE TEST RIG

CRACK COMBUSTION CHAMBER

The major components of the crack combustion chamber used during this reporting period are essentially the same as those described previously in the last annual report.[1] The exit nozzle, which controls the peak chamber pressure and affects the chamber pressurization rate, were

---

[9]K. J. Bathe, E. L. Wilson, and R. H. Iding. *NONSAP: A Structural Analysis Program for Static and Dynamic Response of Nonlinear Systems.* University of California, Berkely, CA, February 1974. (USESM 74-3, publication UNCLASSIFIED.) (Also NTIS PB-231 112.)

[10]T. Y. Chang, S. Prachuktam, and M. Reich. "Assessment of a Nonlinear Structural Analysis Finite Element Program (NONSAP) for Inelastic Analysis," presented at *ASME-Energy Technology Conference, 18-23 September 1977, Houston, Texas.* (ASME Paper 77-PVP-10.)

[11]T. Y. Chang and S. Prachuktam. *NFAP, A Nonlinear Finite-Element Analysis Program.* University of Akron, Akron, Ohio, October 1976. (Report No. SE 76-3, publication UNCLASSIFIED.)

previously made of stainless steel. After several test firings, the exit nozzle throat area was enlarged due to metal erosion; usually, the area became noncircular, which introduces difficulties in achieving reproducible test runs. The metal erosion problem has been alleviated by fabricating the nozzle from titanium which is less sensitive to metal erosion. The titanium nozzle has shown no metal erosion in test firings done to date.

IGNITION SYSTEM

There are two major drawbacks of the previously used methane-oxygen igniter. First, the gaseous ignition system produces ignition with a long ignition delay time followed by a very short flame spreading interval. In order to observe the flame spreading phenomena along the crack with a proper framing rate, one must either use a very high footage of film or be able to control the initial starting of the camera to incorporate the long ignition delay. The use of high footage films is extremely expensive and the control of the camera start time would be very difficult to achieve. Second, as described in Ref. 1, the rocket chamber pressurization rate was found to be an important variable in influencing the flame propagation rate inside propellant cracks. The gaseous igniter can produce only relatively low chamber pressurization rates. In order to simulate the conventional pressuriztion rates during rocket motor ignition transient or to simulate the case of submerged cracks, it is desirable for the igniter to be capable of obtaining broad ranges of chamber pressurization rates.

Based on these requirements, it was decided to develop a more versatile ignition system than the previously used gaseous ignition system. Prior to the development of a successful ignition system, a variety of igniter designs were tested and found to be inadequate during the early development phase.

Numerous experiments were conducted with an igniter which used a Mk 125 ignition element. This igniter produced an undesirable amount of metallic debris and generated uncontrollably large pressure excursions in the small volume near the entrance to the propellant crack. Consequently, the Mk 125 igniter design was abandoned, and a different ignition system was designed which would permit testing with a variety of propellant charges.

As schematically described in Figure 1, the igniter uses a solenoid-actuated firing pin to initiate a percussion element (FA-34) which ignites propellant shavings in the booster chamber and the propellant in the main igniter chamber. A variety of gun propellants (WC 870, WC 846, M 6, and M 26) and solid rocket propellants (AFRPL nonmetallized AP composite and Navy Propellant Type A) were tested in the main igniter chambers. Only the rocket propellants produced a workable system that could be easily ignited and would not prematurely extinguish.

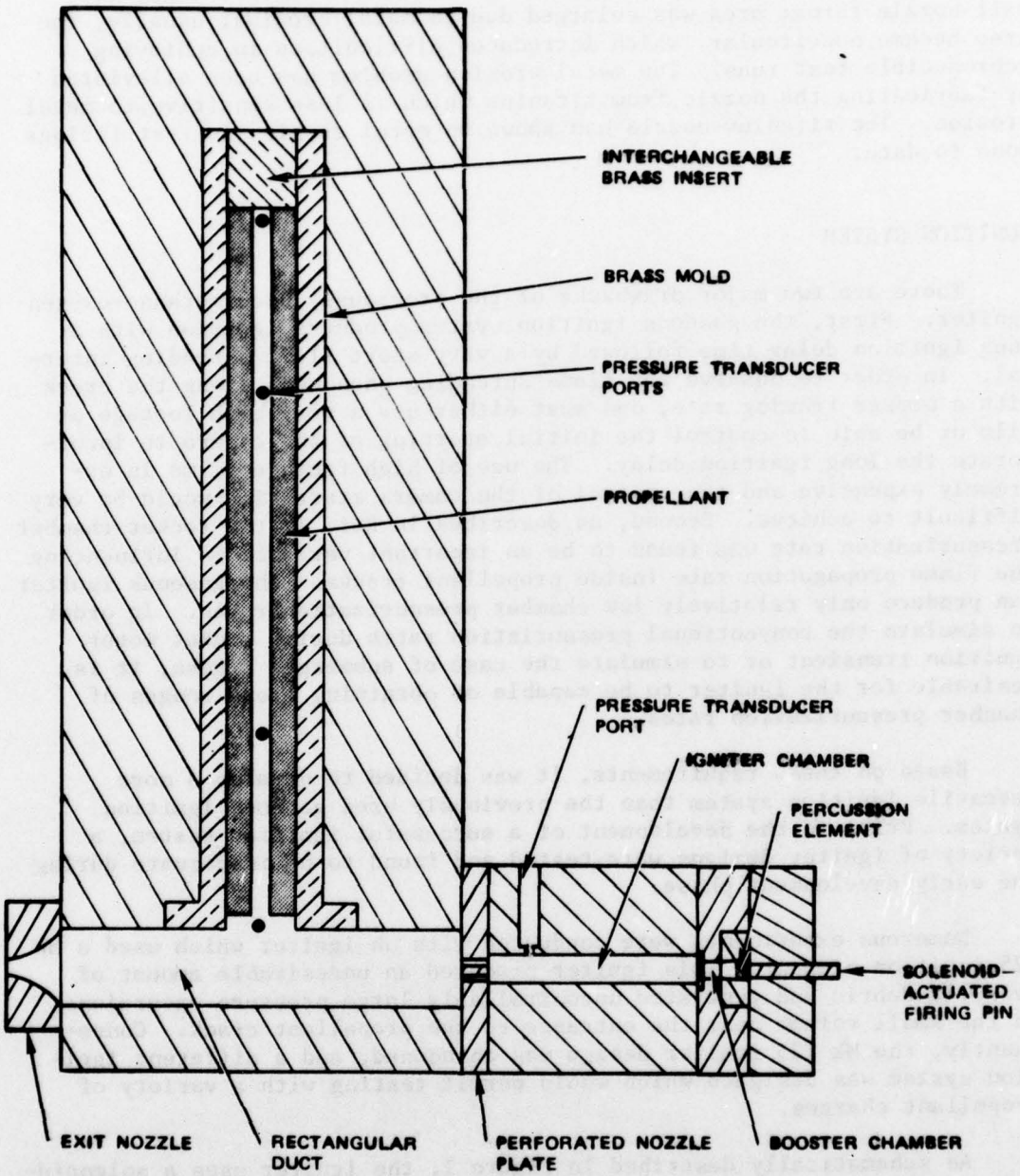

FIGURE 1. Schematic Diagram of Propellant Crack Combustion with the Solid Propellant Igniter System.

Although the propellant shavings were useful in helping the ignition of the propellant charge in the main igniter chamber, it is difficult to control the surface area of the shavings and thus hard to control the igniter pressure pulse. In order to achieve high reproducibility of the pressurization process in the crack combustion chamber, the propellant shavings were deleted from the booster chamber. To facilitate and ensure a successful ignition of the propellant charge in the main igniter chamber, the propellant charge was coated with an igniter paste (Ti-B-$KClO_4$] suggested by Mr. H. B. Mathes of NWC.* This set-up has proven to be successful to generate reproducible pressurization rates, on the order of 10^5 atm/s at the opening of the crack. The initial pressurization rate in the crack combustion chamber can be controlled by varying the igniter charge weight, the area of the inlet perforated nozzle, and the area of the exit nozzle in the combustion chamber. The exploded view of the present igniter system is shown in Figure 2. The complete assembly view of the igniter system mounted together with the crack combustion chamber is shown in Figure 3.

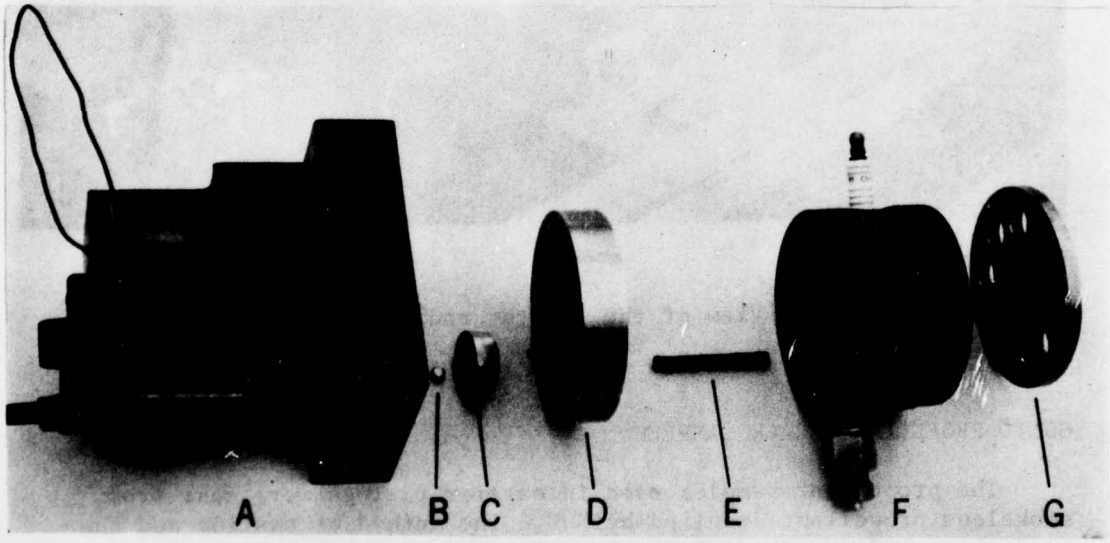

A - Solenoid armature
B - Percussion element
C - Retainer for percussion element
D - Booster chamber
E - Propellant igniter charge
F - Igniter chamber
G - Perforated nozzle plate

FIGURE 2. Exploded View of Solid Propellant Igniter System.

*Personal communication with H. B. Mathes, NWC, 19 July 1977.

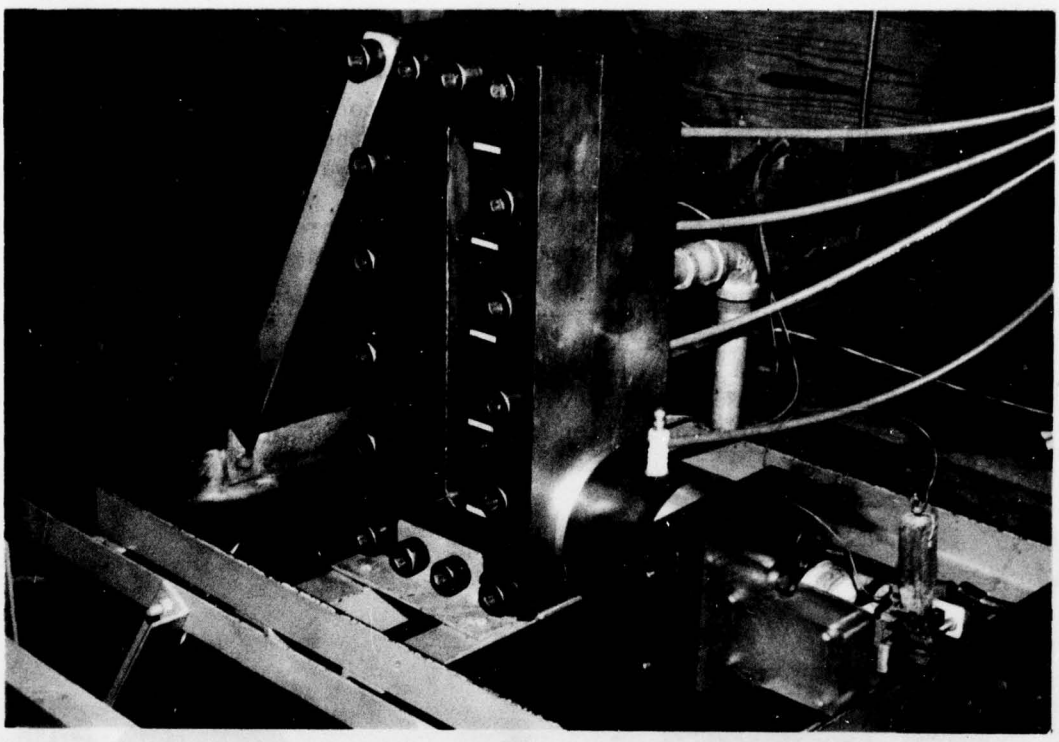

FIGURE 3. Assembly View of the Igniter and Crack Combustion Chamber.

SOLID PROPELLANT CRACK SAMPLES

The propellant samples used in earlier firings were cast from smokeless propellant supplied by NWC. The method of casting and the arrangement of casting mold with teflon-coated mandrel were discussed in the previous annual report.[1] Since the smokeless propellant is very viscous in its liquid state, it is difficult to eliminate bubbles from the cast sample. Therefore, a rubber-based composite propellant, designated as Propellant A, has been used to replace the smokeless propellant in our experimental investigations. Two different mandrel sizes have been used in the casting process; one to form a large crack with an average gap width of 0.52 cm and a length of 20 cm, and the other to form a small crack with an average gap width of 0.10 cm and a length of 15 cm. The case sample for a small crack is shown in Figure 4.

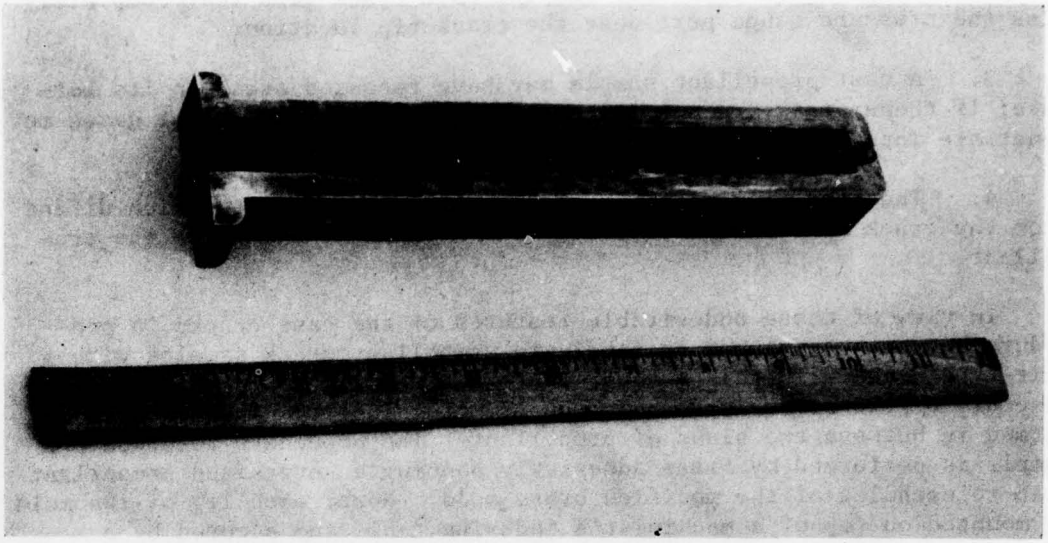

FIGURE 4. Cast Propellant Crack Sample.

Test firings were conducted with the cast samples of both large and small cracks. In these firings, propellant debond at the interface of the sample and the brass mold was observed. The flame propagation along the debond is given in detail in Discussion of Results. The cause for the debond is believed to be due to the bonding weakness at the interface of the two different materials. To reduce the possibility of debond, the propellant specimen was trimmed off at the crack opening and the interface corners of the recessed cavity were reinforced with epoxy. This procedure has proven to be successful in eliminating the debond problem. As a result of recessing the entrance plane of the crack sample, the length of the crack is slightly less than the initially designed mandrel length.

There are several undesirable features of the cast propellant samples:

1. The gap width of the crack is usually nonuniform along the crack length, even though the mandrel is of uniform thickness. The percentage of gap width variation could be as high as 60% for small cracks. It is very unlikely to have crack samples of same initial geometrical configurations; this presents problems in repeating a given experiment.

2. The mandrels may deflect from the centerline during the casting process. This deflection results in the crack gap not aligning with

the pressure gauges. Some cast samples have crack gaps that completely miss the pressure gauge port near the crack tip location.

3. A cast propellant sample may have recessed areas on its surface; if these areas are not filled with epoxy, a flame or hot gases may penetrate into these defect areas.

4. The cast propellant crack has fuel-rich surfaces which differ from the crack surfaces generated by the mechanical damage of the propellant.

In view of these undesirable features of the cast cracks, a procedure has been developed to fabricate propellant crack samples with a slit-type crack. In this method, the brass mold is replaced by the assembly of two brass legs and an upper metal insert. The crack is formed in between two slabs of propellant. The procedure to prepare a sample is performed by first adhesively bonding an oversized propellant slab to each leg of the modified brass mold. Next, each leg of the mold is mounted on top of a machinist's indexing table and secured by a retaining system. The indexing table is attached to a drill press and all exposed surfaces of the propellant slab are precisely cut to the desired dimensions by an end mill (see Figure 5). A low-pressure air line is used during the operation to clear propellant shavings. The shavings are collected and later burnt. The operator of the drill press wears a proximity fire suit as a safety precaution. The final crack configuration is shown in Figure 6.

The slit-type propellant cracks have the advantage of better controlled gap width distributions, thus are more suitable for obtaining a high degree of repeatability. Another advantage of this crack arrangement is the ability to form extremely small gap widths. Also, the length of the crack can be easily varied by changing the length of the upper insert piece. The machined propellant surface is closer to the crack surface generated by mechanical damage of the propellant and, therefore, the surface gasification temperature is that of the propellant rather than the fuel-rich surface.

The slit-type propellant cracks also have the flexibility to study the crack tip ignition phenomena. This can be achieved by adhesively bonding a piece of propellant to the bottom surface of the upper insert piece. A propellant crack sample of this modified configuration is shown in Figure 7.

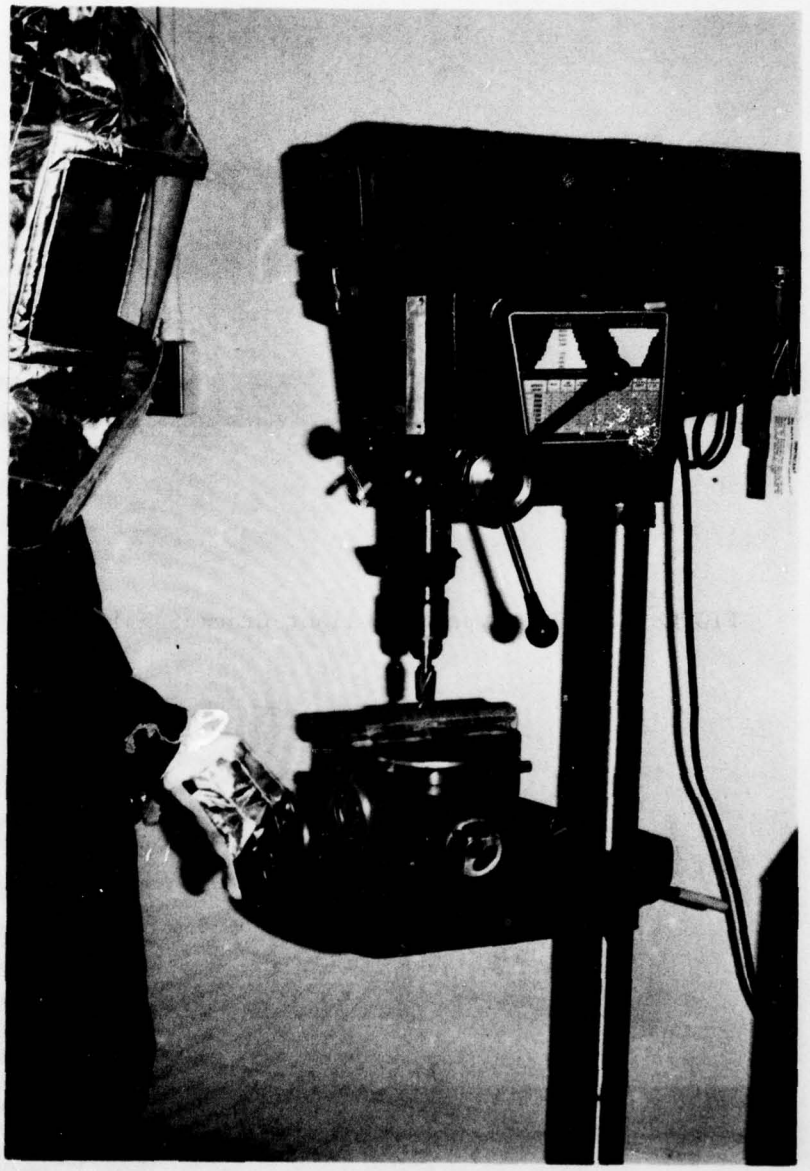

FIGURE 5. Milling of Solid Propellant Slabs to Form Slit-Type Propellant Cracks.

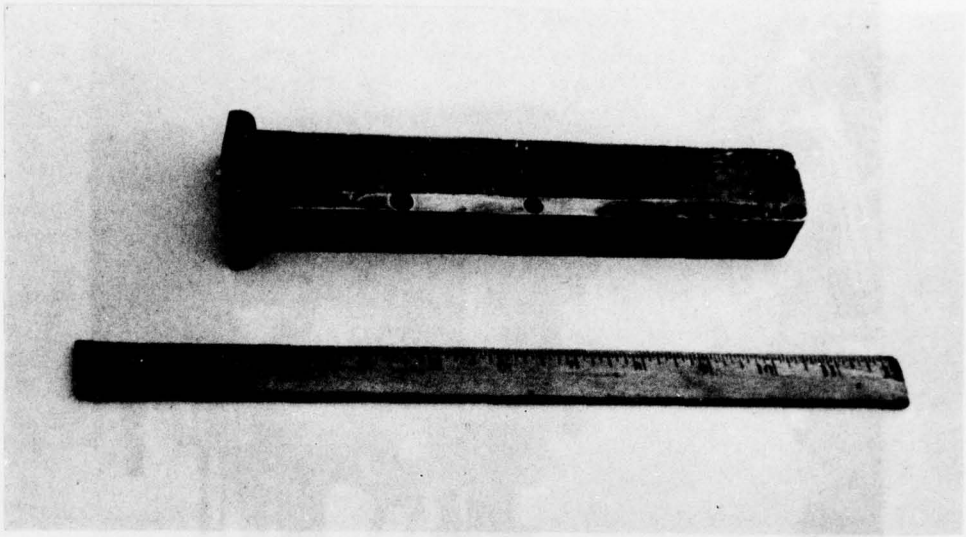

FIGURE 6. Slit-Type Propellant Crack Sample.

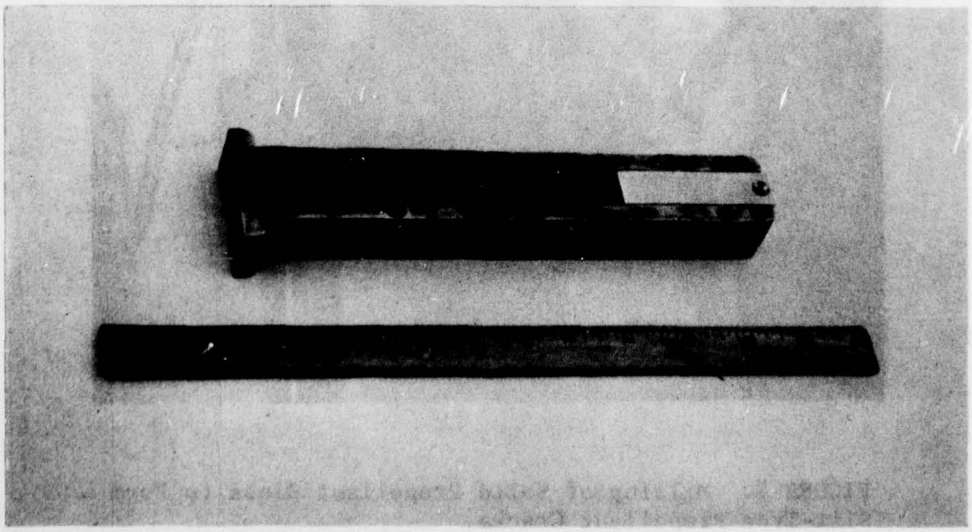

FIGURE 7. Slit-Type Propellant Crack Sample Modified to Study Crack Tip Ignition Phenomena.

In order to check the one dimensionality of the flame spreading process in narrow cracks of various crack width-to-thickness ratios, a new arrangement of the crack configuration has been designed. This new configuration is shown in Figure 8. The crack is formed between a propellant slab slightly regressed below the leg assembly and the inner surface of the plexiglas sacrificial window which is mounted on top of the leg assembly. This type of arrangement allows the observation of the flame spreading process from the front view of the crack surface and thus determines the uniformity of the propagating flame front. Two pressure-time traces will be recorded: one at the opening of the crack and one near the tip of the crack through a slot in the upper insert piece. Although the fabrication of the components for this mold assembly has been completed, the experimental firings were not performed since they were not included in the scope of this reporting period. However, tests will be conducted in the immediate future under the continuing contract.

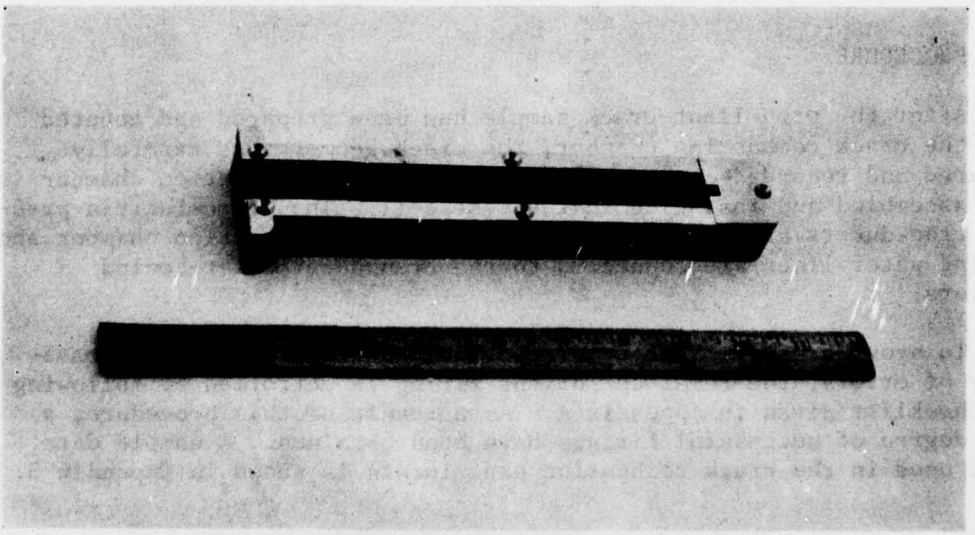

FIGURE 8. Propellant Crack Sample for the Study of One-Dimensionality of the Flame Propagation Phenomena.

CAMERA SYSTEM

A new camera has been incorporated into the data acquisition system to provide for time-correlation between the pressure traces and flame-spreading data. The camera (100' HYCAM) and associated LED drive unit are on loan from NSWC/DL. The event synchronizer circuit of the camera was used to trigger the solenoid-actuated firing pin in the igniter. This special circuit was found to be very advantageous for capturing the flame spread transient and ensuring that the camera was operating at the preselected framing rate prior to ignition. Unfortunately, the 100' HYCAM does not operate at fast enough frame rates (3000 pps maximum with regulated speed control) to give sufficient time resolution of the high-speed flame spread interval. This deficiency has been recently alleviated with a 400' HYCAM camera acquired through an interdepartmental loan at Pennsylvania State University. This camera, which has features similar to those of the 100' HYCAM, can achieve frame rates up to 10,000 pps (5,000 pps for speed regulated mode). The full-frame and accessory half-frame heads of the camera have been modified to interface with a high-precision, externally-driven, LED timing light generator. To facilitate future test firings, a new LED driver unit similar to the one on loan from NSWC/DL has been designed and fabricated. Figure 9 shows an overall view of the filming process.

TEST PROCEDURE

After the propellant crack sample has been prepared and mounted into the crack combustion chamber, the crack geometry is carefully measured and recorded on a data sheet. The crack combustion chamber is then assembled and installed in the test cell. The piezoelectric pressure transducers are then mounted into the crack combustion chamber and cooling water lines are connected to the transducer water-cooled adapters.

To provide maximum safety precautions and to minimize the possiblity of errors, the remainder of the firing is performed by following the checklist given in Appendix A. As a result of this procedure, a high degree of successful firings have been obtained. A sample data sheet used in the crack combustion experiments is shown in Appendix B.

DISCUSSION OF RESULTS

PRESENTATION AND DISCUSSION OF EXPERIMENTAL DATA

During this reporting period, a number of test firings have been conducted to determine the influence of both the solid propellant igniter and the crack geometry on the flame-spreading and pressurization

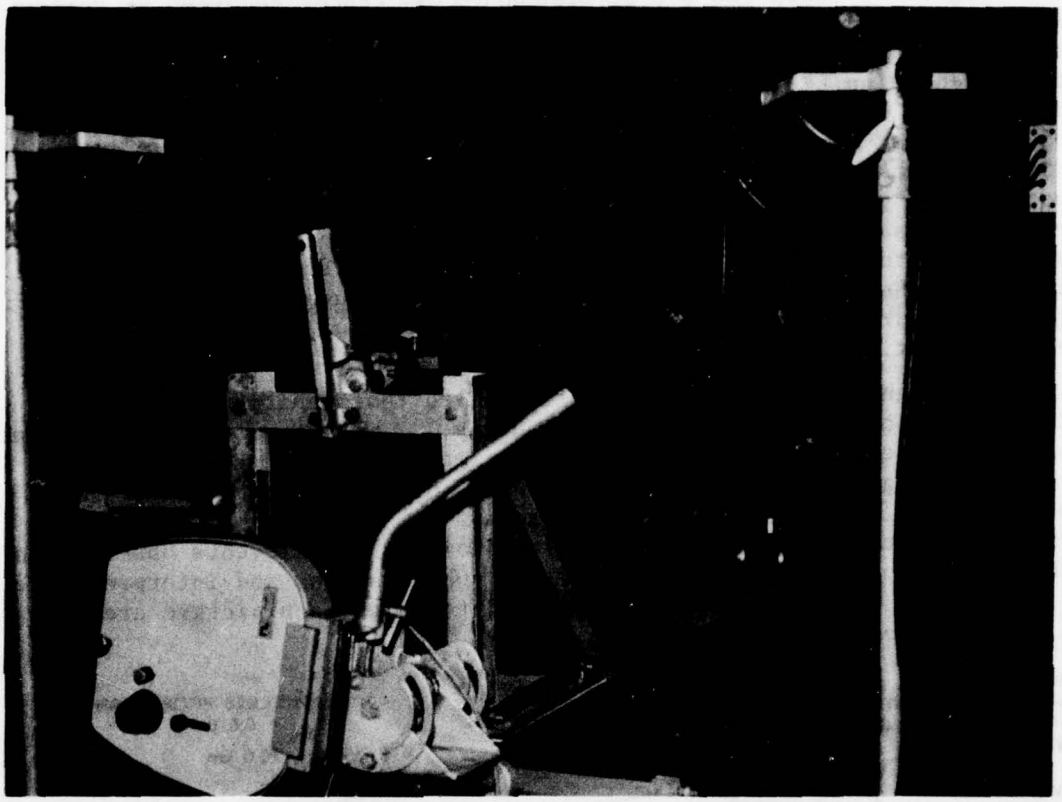

FIGURE 9. Overall View of the Filming Process.

in propellant crack samples. The propellant samples were either cast by NWC or machined to a slit-type crack at Pennsylvania State University. The test runs discussed in this section were all conducted by using the recently developed solid propellant igniter system. The strength of the igniter was varied by changing the propellant charge weight in the igniter chamber.

In the earlier tests, propellant debond at its interface with the brass mold was observed. DNC Test No. 12 represents a typical case of the unplanned debond experiments. In this test the crack sample was cast from smokeless propellant. The gap width was uniform at a value of 0.51 cm and the length of the crack was 20 cm. The igniter system was composed of an FA-34 primer, AF composite propellant shavings as booster, and a rectangular charge of AF propellant with a weight of 2.284 g.

Figure 10 shows the set of pressure-time traces recorded at various locations along the crack. Time-correlation of the pressure and flame spreading data is achieved with the common-time pulse. The pulse was generated by an LED driver when the igniter solenoid was energized. As measured by Gauge 2 (G2), the igniter produced an initial peak pressure of 120 atm at a rate of 1.76×10^5 atm/s in the main chamber of the test rig. The shape of the p-t trace near the first peak of G2 closely matches the profiles obtained from igniter tests with a simulated inert propellant sample. This implies that the initial pressure pulse is solely due to the igniter output. During this initial pressure pulse interval, the pressurization rates differ from gauge-to-gauge. All gauge pressures rise, due to gasification processes, as the combustion process continues until a second peak is reached.

The high-speed film (2540 pps) revealed that ignition occurred at the opening of the debond at approximately 1.2 ms after the first glimpse of hot igniter gas in the chamber. The ignition front then proceeded rapidly along a developing debond between the propellant and the brass mold. Flame spreading in the crack occurs at a later time. Certain frames from this film were selected to show important events observed in the combustion process (see Figure 11). Observations and interpretations of the combustion phenomena associated with each picture are listed in Table 1.

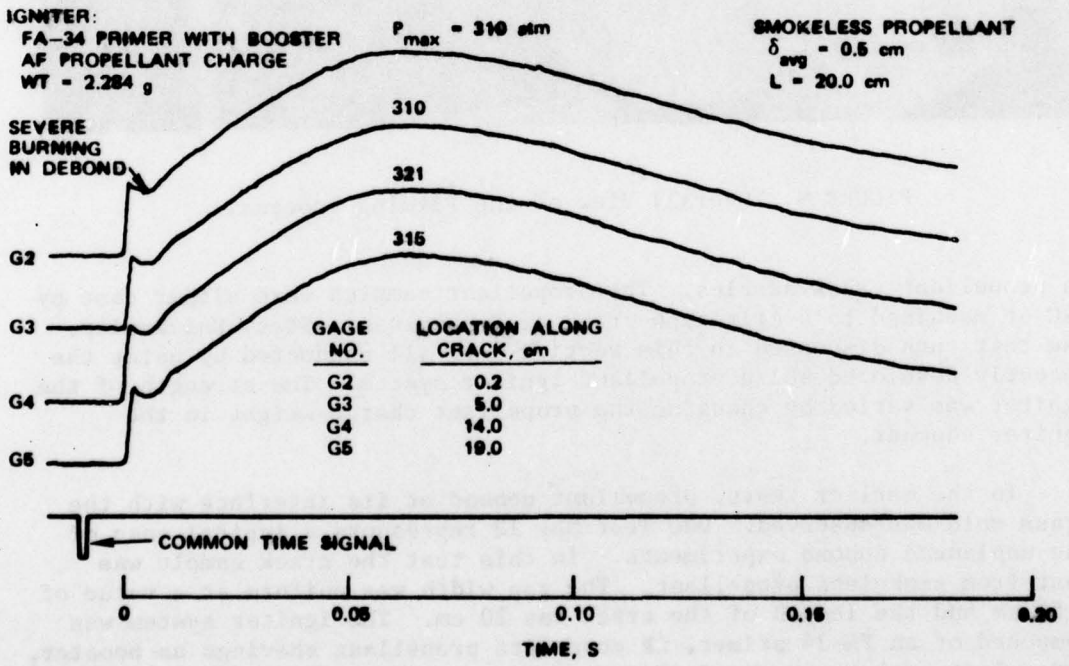

FIGURE 10. Experimental Pressure-Time Traces from DNC Test No. 12.

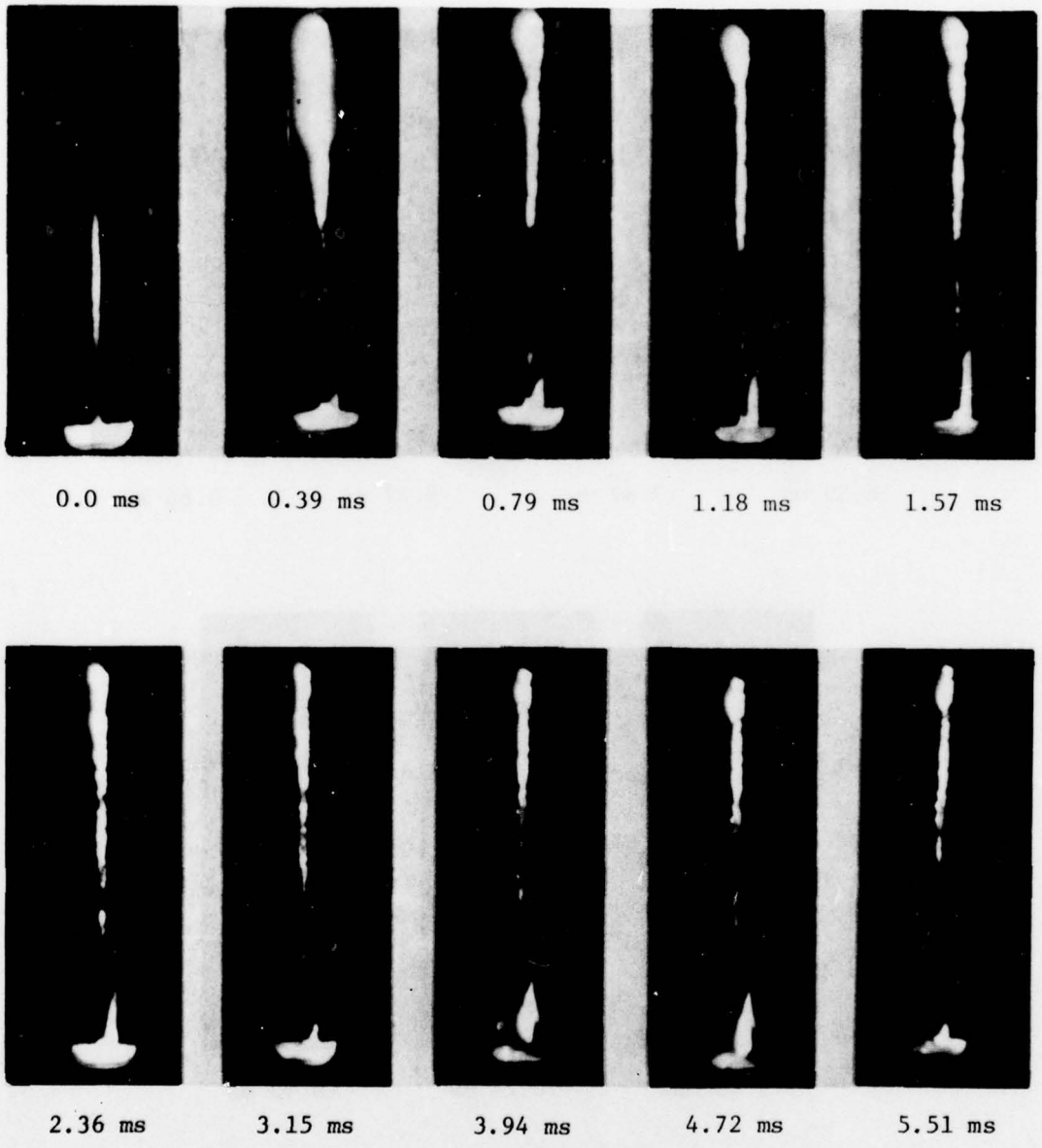

FIGURE 11. Motion Pictures of the Ignition and Combustion Phenomena in a Solid Propellant Crack with Unplanned Debond in DNC Test No. 12.

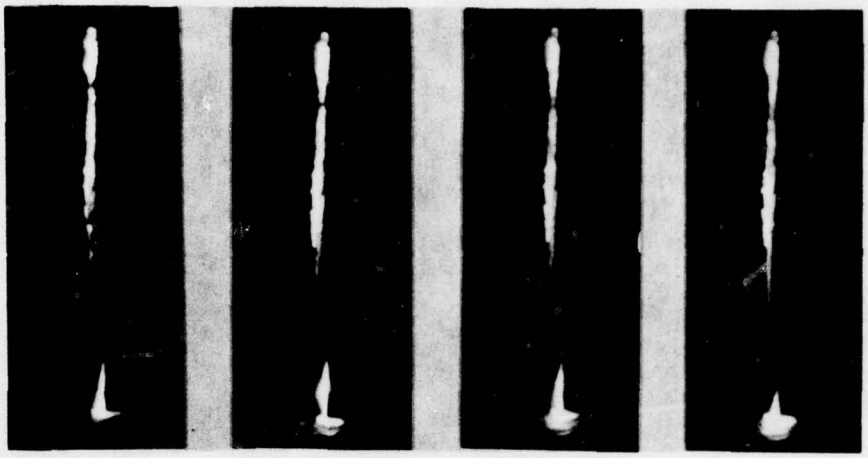

6.69 ms 7.87 ms 8.27 ms 8.66 ms

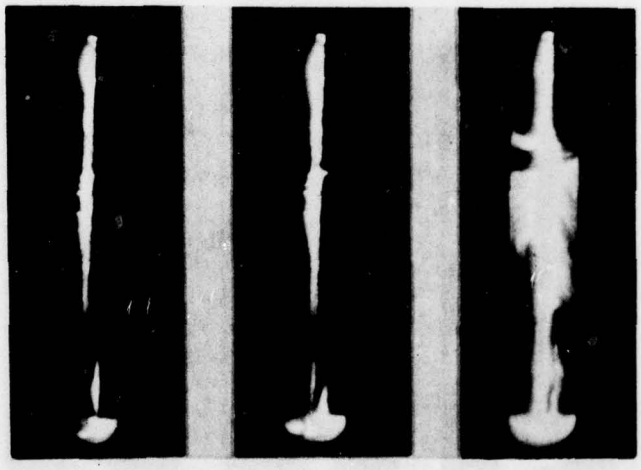

9.45 ms 10.24 ms 18.90 ms

FIGURE 11. (Contd.)

TABLE 1. Physical Interpretation of the Film of DNC Test No. 12.

Picture No.	Time, ms	Observations and interpretations
1	0.0	Hot igniter gas enters the rectangular duct in the bottom of the main chamber and begins to penetrate into the crack
2	0.39	Brightness in the debond region showing penetration of hot gases into the debond crack
3	0.79	The developing debond between the propellant and the brass mold closes the crack opening
4	1.18	Possible ignition near the opening of the debond
5	1.57	There is a propagation of debond crack
7	2.36	Gas pressure starts to open the crack and close the debond
9	3.15	Extinction occurs in a part of the debond due to closure of that portion of the debond
11	3.94	Severe burning in the debond once again closes the crack opening
13	4.72	Severe burning continues in the debond
15	5.51	The crack entrance begins to open
18	6.69	The crack is closed
21	7.87	The crack is open, yet there is still burning in the debond
22	8.27	The crack is closed
23	8.66	The crack is open
25	9.45	The crack is open, yet there is still burning in the debond
27	10.24	There is severe burning in the crack. Gas starts to flow into the gap between the propellant sample and the chamber window
49	18.90	The debond piece becomes thin due to burning on both surfaces

The next test firing data selected for discussion was DNC Test No. 16. The crack sample used was cast by NWC from Type A propellant. The average gap width was 0.14 cm and the length of the crack was 14.24 cm. The igniter was the same as DNC Test 12 except the propellant charge weight for this test firing was 1.925 g. The debond problem was eliminated by utilizing the method described in the section entitled "Experimental Set-Up of the Test Rig."

Figure 12 shows the measured pressure-time traces along the crack. The average pressurization rate at G2 before reaching the peak pressure is approximately 0.7×10^5 atm/s. It is interesting to note that at this high pressurization rate, the pressure irregularities at downstream gauge locations immediately follow the first discernible pressure rate at G2. These irregularities are believed to be caused by strong wave propagation and reflection phenomena inside the crack. These pressure irregularities continue to appear until the pressure peak region is over. It is also important to note that the pressure trace at each gauge location displays only one pressure peak region.

The pictures showing the important gas penetration and flame spreading event are given in Figure 13. The detailed observations of these pictures are listed in Table 2. Generally speaking, the flame spreading information obtained in this firing seems to suggest that when the compression wave generated by the igniter system is too strong, the region near the crack tip may be ignited earlier than the region closer to the entrance of the crack. This phenomena produces flame spreading in the reversed direction near the crack tip which in turn can lead to the convergence of two propagating flame fronts.

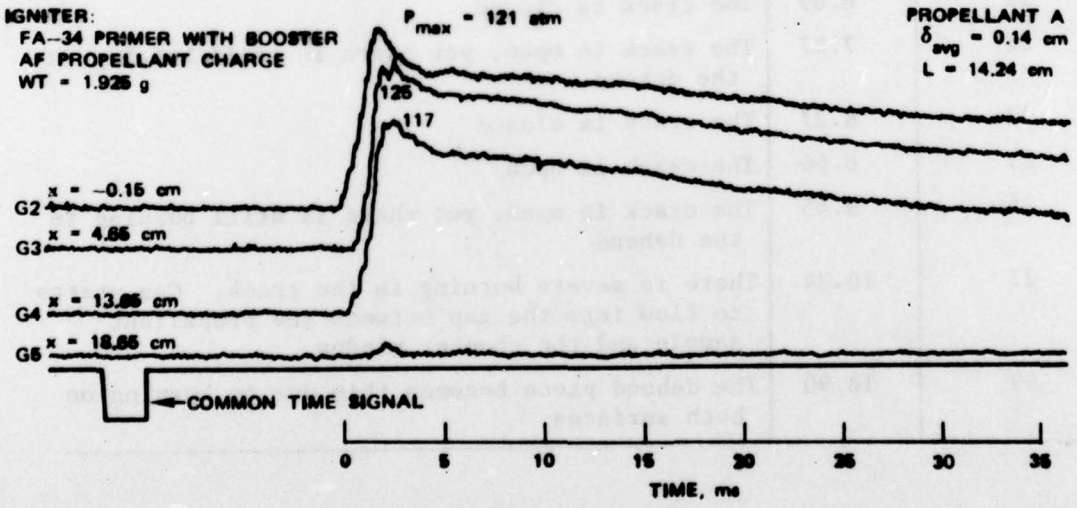

FIGURE 12. Experimental Pressure-Time Traces from DNC Test No. 16.

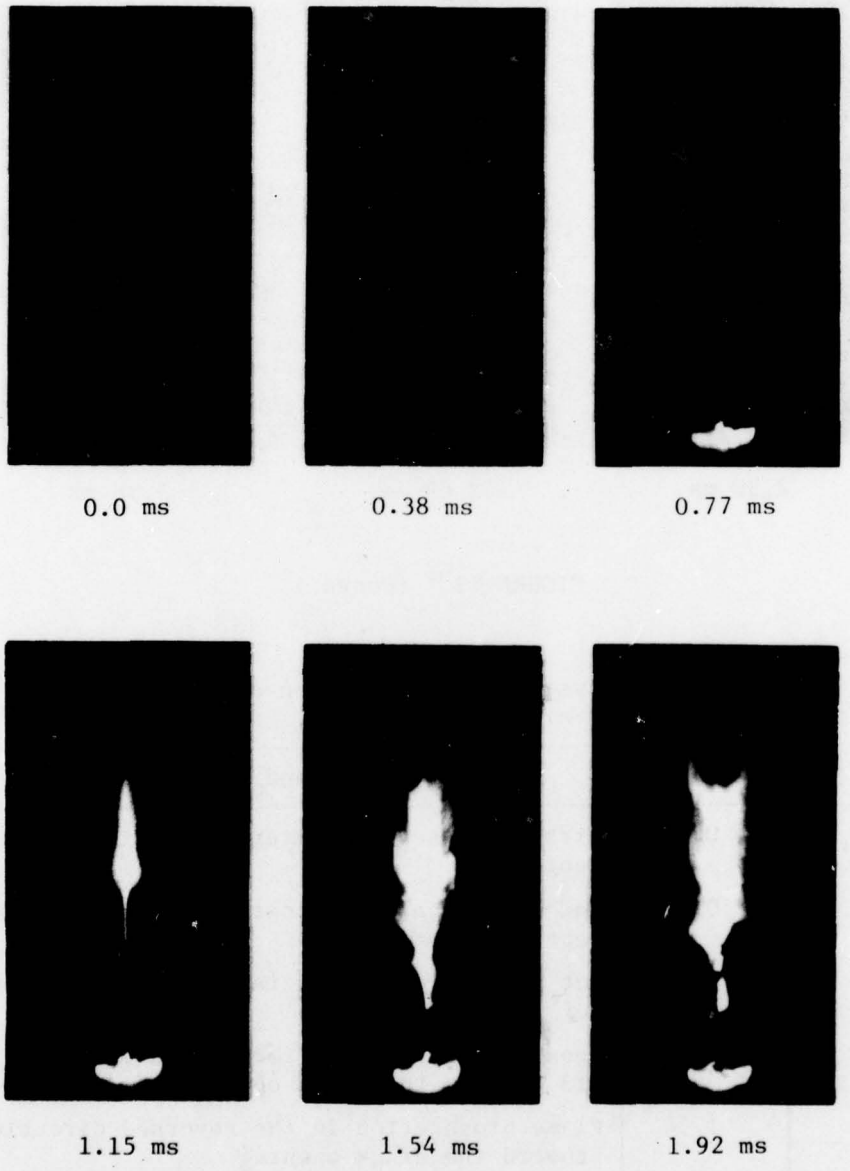

FIGURE 13. Motion Pictures of the Ignition and Combustion Phenomena in a Solid Propellant Crack of DNC Test No. 16.

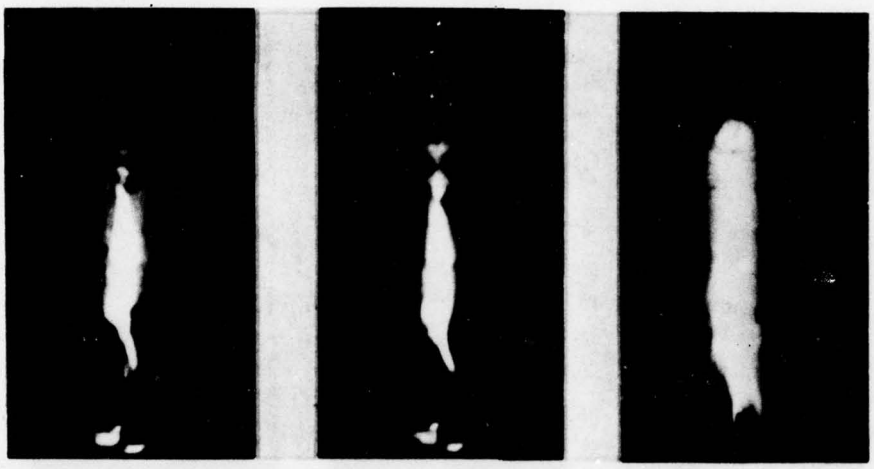

2.30 ms 2.69 ms 5.38 ms

FIGURE 13. (Contd.)

TABLE 2. Physical Interpretation of the Film of DNC Test No. 16.

Picture No.	Time, ms	Observations and Interpretations
1	0.0	First glimpse of igniter gas at the crack entrance
2	0.38	Hot gases start to penetrate the crack near the entrance
3	0.77	Hot gases are noticed in the downstream portion of the crack
4	1.15	Possible ignition in the region between 9 to 13 cm from the crack opening
5	1.54	Flame propagation in the reversed direction toward the crack opening
6	1.92	Severe burning near the center of the crack
7	2.30	The area at the crack entrance is substantially reduced
8	2.69	Severe burning inside the crack
15	5.38	After severe burning has continued for 2 ms, the crack entrance is enlarged again

The compression wave generated ignition involves a new mechanism of ignition other than the conventional ignition caused by convective heating of the propellant surface. Currently, this new mechanism has not been considered in the crack combustion model; therefore, the convergent flame propagation phenomena cannot be predicted by our computer code. This new mechanism of ignition in the authors' opinion deserves future investigations.

In DNC Test No. 18 the propellant sample was again cast by NWC from Type A propellant. The average gap width was 0.16 cm and the crack length was 14.73 cm. The same igniter was used but with a propellant charge weight of 1.966 g. The pressure-time traces are shown in Figure 14. The pressurization rate of G2 at the onset of pressurization is approximately 2.2×10^5 atm/s which is nearly three times the rate of DNC Test No. 16. Again, the strong pressure irregularities following the first discernible pressure rise are noticed in the downstream gauges. There are mild second peak pressures reached at time considerably longer than initial pressurization time.

The pictures describing the observed gas penetration, ignition, and flame propagation phenomena are given in Figure 15. The interpretations of these pictures are given in Table 3. Similar to DNC Test No. 16, the tip region seems to be ignited before the flame propagates from the crack entrance to the tip, resulting in flame propagation in both directions.

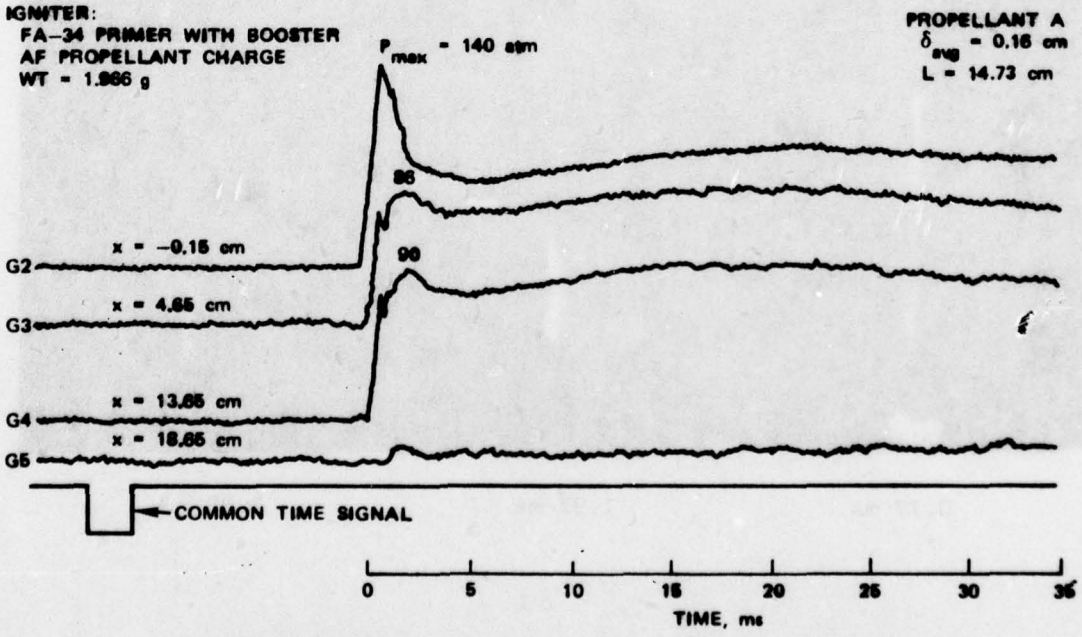

FIGURE 14. Experimental Pressure-Time Traces from DNC Test No. 18.

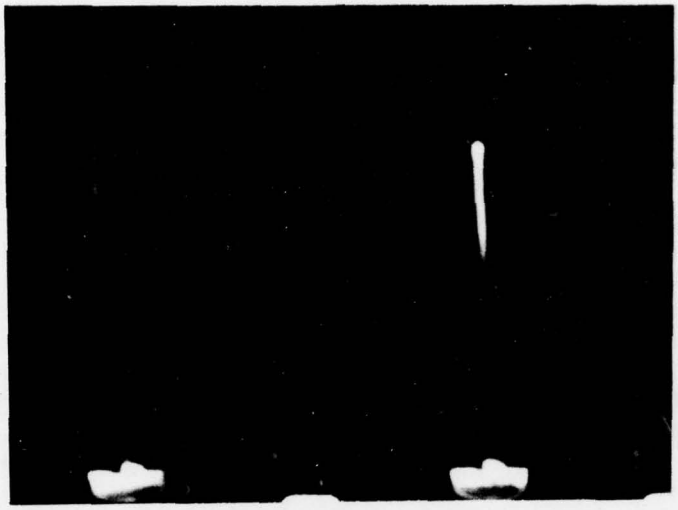

0.0 ms 0.38 ms

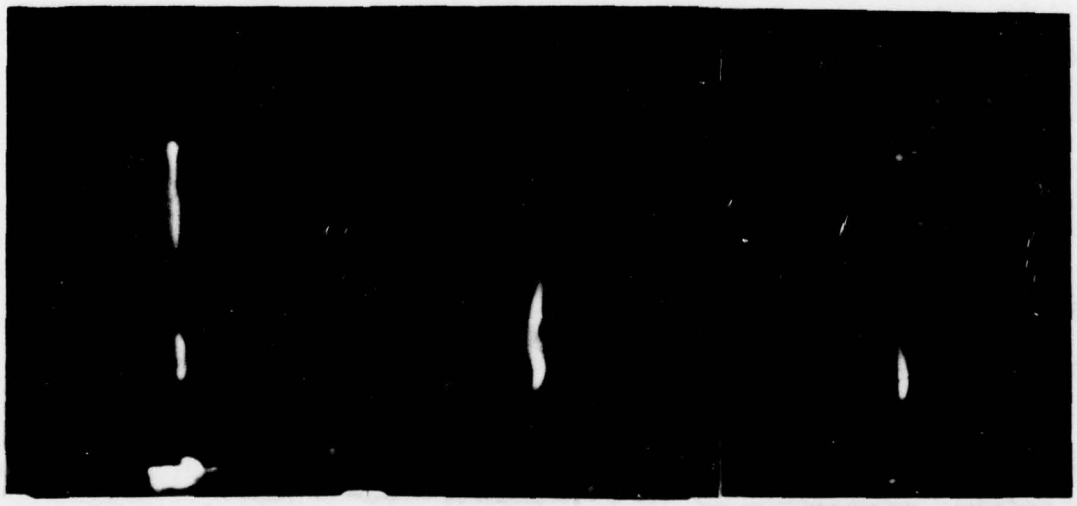

0.77 ms 1.92 ms 3.08 ms

FIGURE 15. Motion Pictures of the Ignition and Combustion Phenomena in a Solid Propellant Crack of DNC Test No. 18.

TABLE 3. Physical Interpretation of the Film of DNC Test No. 18

Picture No.	Time, ms	Observations and interpretations
1	0.0	Hot igniter gases enter the combustion chamber and start to penetrate the crack
2	0.38	Hot gases are noticed near the crack tip indicating possible ignition in this region.
3	0.77	Flame propagates in both directions
6	1.92	Severe burning near the region 3.5 cm from the crack opening
9	3.08	The crack tip region and the 3.5 cm region are burning most severely, while other regions remain less intense

DNC Test No. 22 was conducted by using the slit-type crack sample fabricated from Propellant A. The gap width of the crack was a uniform value of 0.19 cm and the length was 14 cm. The igniter consisted of an FA-34 primer and an igniter charge of Propellant A at a weight of 2.066 g which was coated with Ti-B-$KClO_4$ ignition paste. Since the igniter charge was made of Propellant A rather than the more energetic AF composite propellant and also there were no propellant shavings in the booster chamber, the initial chamber pressurization rate was much lower than the cases discussed earlier. The initial pressurization rate for this test was 0.166×10^5 atm/s.

The pressure-time traces at the crack opening and the crack tip for this test firing are shown in Figure 16. Due to the fact that the crack gap width is larger than those in DNC Test No. 16 and 18, and also the initial pressurization rate for this test is much lower, the downstream gauge does not have the pressure irregularities recorded in the two previously discussed tests. The pressure gradient along the crack is very small even in the initial pressurization interval; this is consistent with the theoretical findings for cracks of relatively large gap widths ignited with relatively low chamber pressurization rates.

The pictures showing the important events occurring in the time interval of interest are shown in Figure 17. The interpretations of the observed phenomena for these pictures are listed in Table 4. The advancement of the flame front can be seen clearly from these pictures and the flame deceleration near the closed end of the crack agrees with the observations made separately by Belyaev, et al. and Taylor.[4,12]

[12] J. W. Taylor. "The Burning of Secondary Explosive Powders by a Convective Mechanism," *Trans. Farad. Soc.*, Vol. 58 (1962), p. 561.

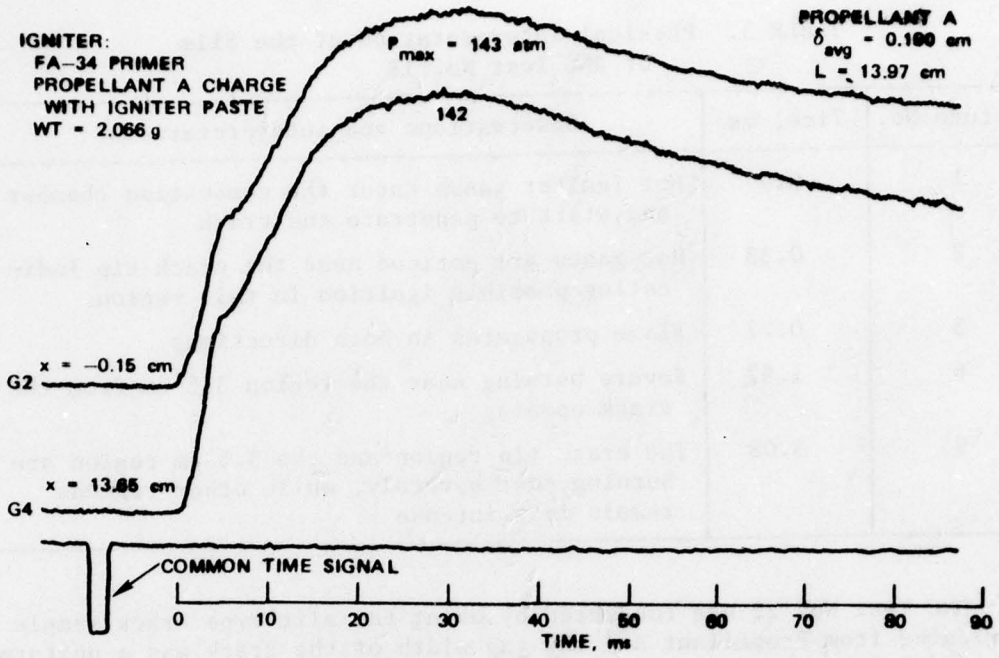

FIGURE 16. Experimental Pressure-Time Traces from DNC Test No. 22.

COMPARISON OF THEORY WITH EXPERIMENT

Figure 18 shows a typical set of experimental and theoretical p-t traces. The experimental p-t traces shown were measured from DNC Test No. 21. The crack specimen for this test firing was made of propellant Type A cast by NWC. The length of the crack was 14.6 cm and the gap width at the crack opening was 0.089 cm, increasing gradually to 0.140 cm at the tip. The theoretical p-t traces shown were obtained from the crack combustion code using the input data listed in Table 5. Time zero in Figure 18 is defined as the time corresponding to the first glimpse of igniter gas on the high-speed film.

Several special features were observed by comparing the experimental p-t traces measured at various locations. The first discernible pressure rise in G2 occurs very shortly ($\Delta t < 0.2$ ms) after the first glimpse of hot igniter gas. Each gauge measures two peaks; the first peak is essentially caused by the discharge of the igniter material and the second peak is caused by the burning inside the propellant crack. Although the pressures at the first peak do not differ significantly for the three gauge locations, the rates of pressurization to achieve the

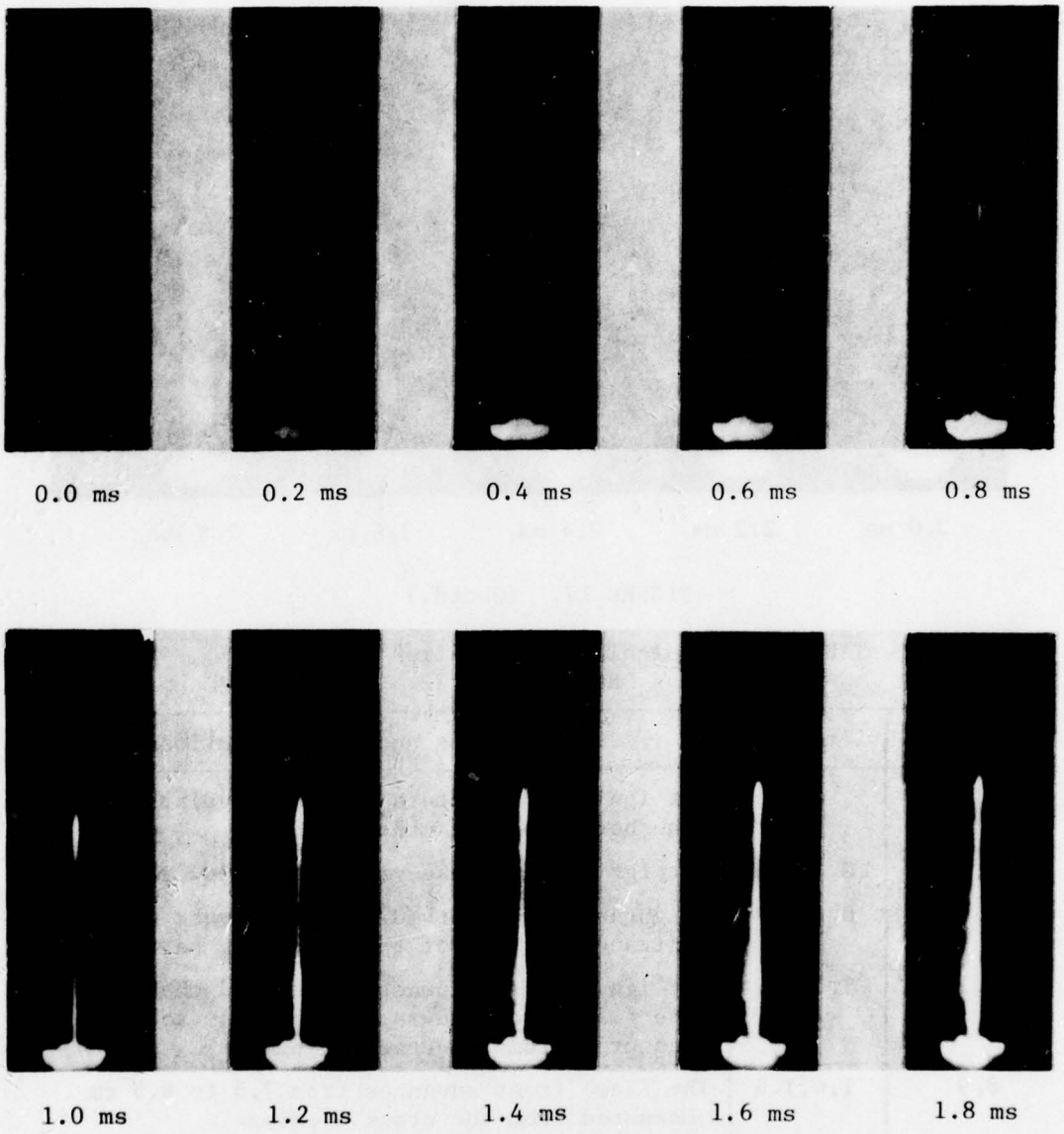

FIGURE 17. Motion Pictures of the Ignition and Combustion Phenomena in a Solid Propellant Crack of DNC Test No. 22.

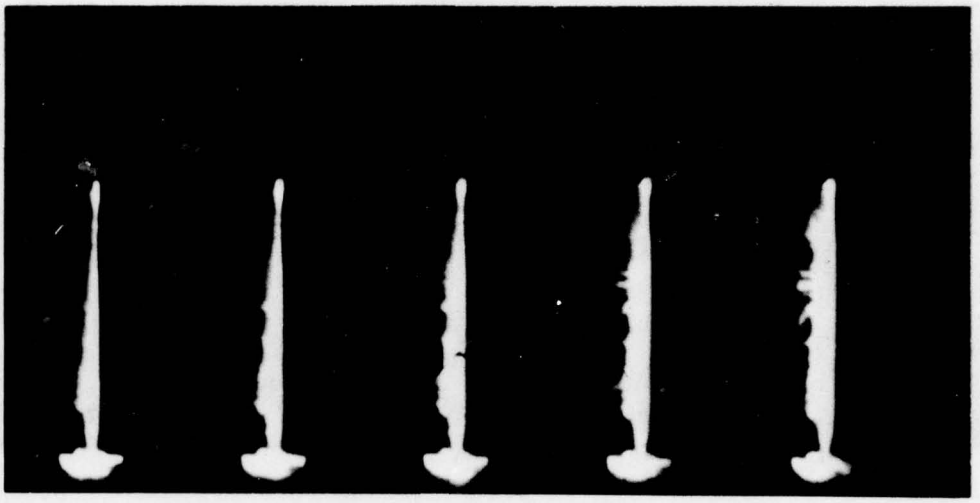

2.0 ms 2.2 ms 2.4 ms 2.6 ms 2.8 ms

FIGURE 17. (Contd.)

TABLE 4. Physical Interpretation of the Film of DNC Test No. 22.

Picture No.	Time, ms	Observations and interpretations
1	0.0	Hot igniter gas enters the rectangular duct in the bottom of the main chamber
2,3	0.2,0.4	Hot igniter gas penetrates into the crack
4,5	0.6,0.8	Brightness is observed near the crack tip. The entrance portion of the crack may be ignited
6,7	1.0,1.2	Hot igniter gases penetrate toward the crack tip, The flame front advances from 5 cm to 6.5 cm measured from the crack opening
8,9	1.4,1.6	The flame front advances from 7.5 to 8.5 cm measured from the crack opening
10,11	1.8,2.0	Flame propagation continues. The flame front advances from 10 to 11 cm measured from the crack opening
12,13	2.2,2.4	Brightness near the crack tip suggests ignition in this region. Flame front is decelerated near the crack tip region but still advances from 11.5 to 12 cm
14,15	2.6,2.8	High intensity gas fills the entire length of the crack

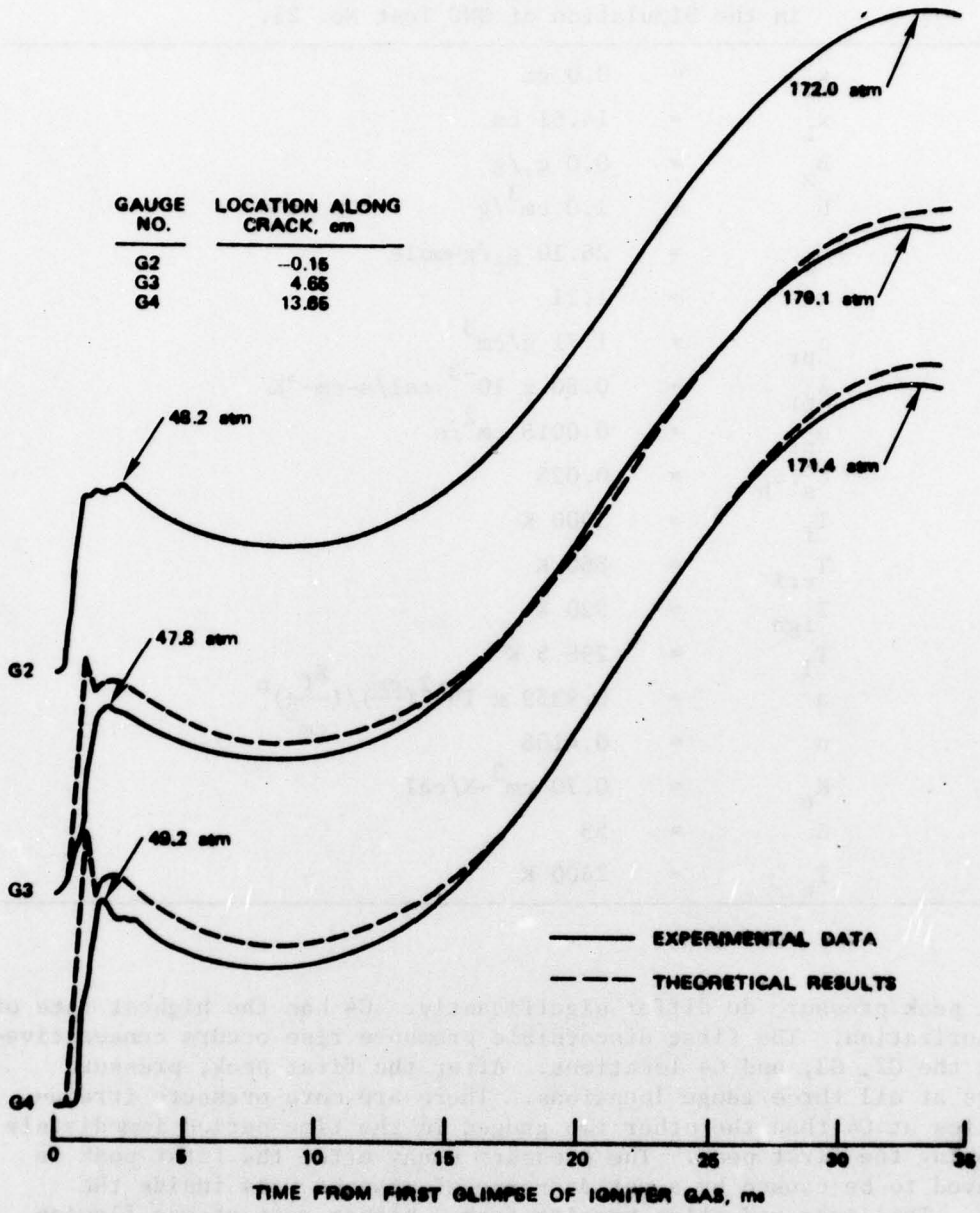

FIGURE 18. The Comparison of Experimentally Measured and Theoretically Calculated p-t Traces for DNC Test No. 21.

TABLE 5. Computer Program Input Variables in the Simulation of DNC Test No. 21.

x_p	=	0.0 cm
x_L	=	14.61 cm
B_x	=	0.0 g_f/g
b	=	1.0 cm^3/g
M_w	=	26.10 g_f/g-mole
γ	=	1.21
ρ_{pr}	=	1.71 g/cm^3
λ_{pr}	=	0.80 x 10^{-3} cal/s-cm-°K
α_{pr}	=	0.0018 cm^2/s
ε_s/d_h	=	0.025
T_f	=	3000 K
T_{cri}	=	860 K
T_{ign}	=	920 K
T_i	=	298.5 K
a	=	0.9359 x $10^{-2}(\frac{cm}{s})/(\frac{g_f}{cm^2})^n$
n	=	0.4108
K_e	=	0.70 cm^3-K/cal
β	=	53
T_c	=	2400 K

first peak pressure do differ significantly. G4 has the highest rate of pressurization. The first discernible pressure rise occurs consecutively at the G2, G3, and G4 locations. After the first peak, pressure decays at all three gauge locations. There are more pressure irregularities at G4 than the other two gauges in the time period immediately following the first peak. The pressure decay after the first peak is believed to be caused by a net decrease of gaseous mass inside the crack. This mass reduction results from a higher rate of gas flowing out of the crack than the rate of gasification of propellant inside the crack. The pressure differences between various locations along the crack become smaller and smaller as the second peak is approached. After the second peak, the pressure decays continuously due to the burnout of the propellant sample.

The theoretical p-t traces, shown as dashed lines in Figure 18, are in good qualitative agreement with the experimental results. The time corresponding to the first discernible pressure rise at G2, G3, and G4 increases consecutively. Similar to the experimental traces, the calculated initial pressurization rates differ significantly from each other at the three gauge locations. The pressurization rate at G4 is much higher than the rate of pressurization at the opening of the crack. Also, the calculated p-t traces display pressure irregularities shortly after the first peak near the crack tip. These spikes are due to complicated compression wave phenomena near the crack tip region. Furthermore, in the same manner as the experimental pressure traces, the theoretically calculated pressure distribution along the crack becomes more uniform as the second peak is approached.

In spite of the qualitative similarities discussed above, there is some quantitative disagreement between theory and experiment. The calculated pressures at G3 and G4 are higher than the experimentally measured pressure for a large portion of the time period being examined. The theoretically calculated first discernible pressure rise at G4 occurs before the experimentally observed time. Also, the calculated first peaks for G3 and G4 are greater than the experimentally measured values.

The quantitative disagreements between theory and experiment can be caused by several factors which are not considered in the present model. The current version of the crack combustion code does not account for any mechanical deformation of the crack. The initial pressure pulse from the igniter into the rectangular duct in the bottom of the main combustion chamber could mechanically push the bottom surface of the propellant specimen inward and thereby decrease the crack gap width near the crack opening. Based upon an incompressible assumption, mechanical deformation of the solid propellant can reduce the crack gap width by 50%. This decrease in flow area would result in increased flow resistance into the crack. The flow rate of penetrating gases is reduced by both a decrease in flow area and a decrease in discharge coefficient. The change of propellant contour near the crack opening may substantially reduce the discharge coefficient. If the crack combustion code considered the mechanical deformation of the propellant, then the first discernible pressure rise at the tip would occur at a later time. Also, if the compressibility of the solid propellant was considered in the model, a lower pressure would be obtained in the crack. This indicates the necessity of coupling the crack combustion code with a structure analysis program.

In general, the theoretical results obtained from the crack combustion code are in good qualitative agreement with experimental observation. Although the detailed quantitative comparison of the theoretical results with experimental data showed noticeable differences, the calculated pressure-time traces and the pressurization rates after the

first discernible pressure rise are in reasonable agreement with the data. It is our belief that quantitative match would be improved after coupling the crack combustion code with the structure analysis program (NONSAP).

Figure 19 describes the pressure distribution along the crack at various times. Due to the initial pressurization caused by the igniter, the pressure at the crack opening is greater than that near the crack tip. The pressure gradients at times less than 1 ms are favorable for the penetration of hot gases into the propellant crack. Between 1 ms and 1.25 ms, there is a substantial increase in pressure in a large portion of the crack. This increase is caused by the gasification of propellant inside the crack. The accumulation of gases inside the crack produces a reverse pressure gradient near the crack opening. The product gases are driven out of the crack by the reverse pressure gradient. The outflow of product gases causes a decrease in pressure inside the crack. This is why there are valleys on the p-t traces shown in Figure 18. At the same time, the outflow of product gases greatly decelerates the flame spreading process at the center of the crack.

The calculated locus of ignition front is superimposed as a dashed line in Figure 19. The locus of ignition front indicates rapid flame spreading from the crack opening to 7.7 cm. The flame spreading abruptly decelerates near the center of the crack due to the reason given above. Additional explanation of the flame deceleration is given below in the discussion of the calculated velocity distributions.

The flame spreading and combustion phenomena for DNC Test No. 21 were recorded with a 16-mm high-speed motion picture camera at an average rate of 5100 pps. A number of frames from this film were selected to show the important events in the overall combustion process (see Figure 20). A description of the observed phenomena is given in Table 6. Similar to the theoretical results, the ignition front advances at a high speed through the first half of the crack length and then the flame front becomes stationary near the center of the crack.

Figure 21 shows the calculated gas velocity profiles that exist in the crack at various times. At the time of 0.5 ms the hot gases are flowing into the crack at a high velocity because of a favorable initial pressure gradient. At 1 ms the velocity of the inflowing gases decreases as the pressure gradient at the crack opening decreases. As the flame front progresses along the crack, the resultant gasification processes cause the pressure gradient at the entrance of the crack to reverse. At 2 ms, the product gases are driven out of the crack by the reversed pressure gradient. The decrease in velocity of the outflowing gases between 6 and 10.5 ms is probably due to the increase in port area at the crack entrance which will be discussed later. During the entire pressurization process, the gas velocity near the closed end of the

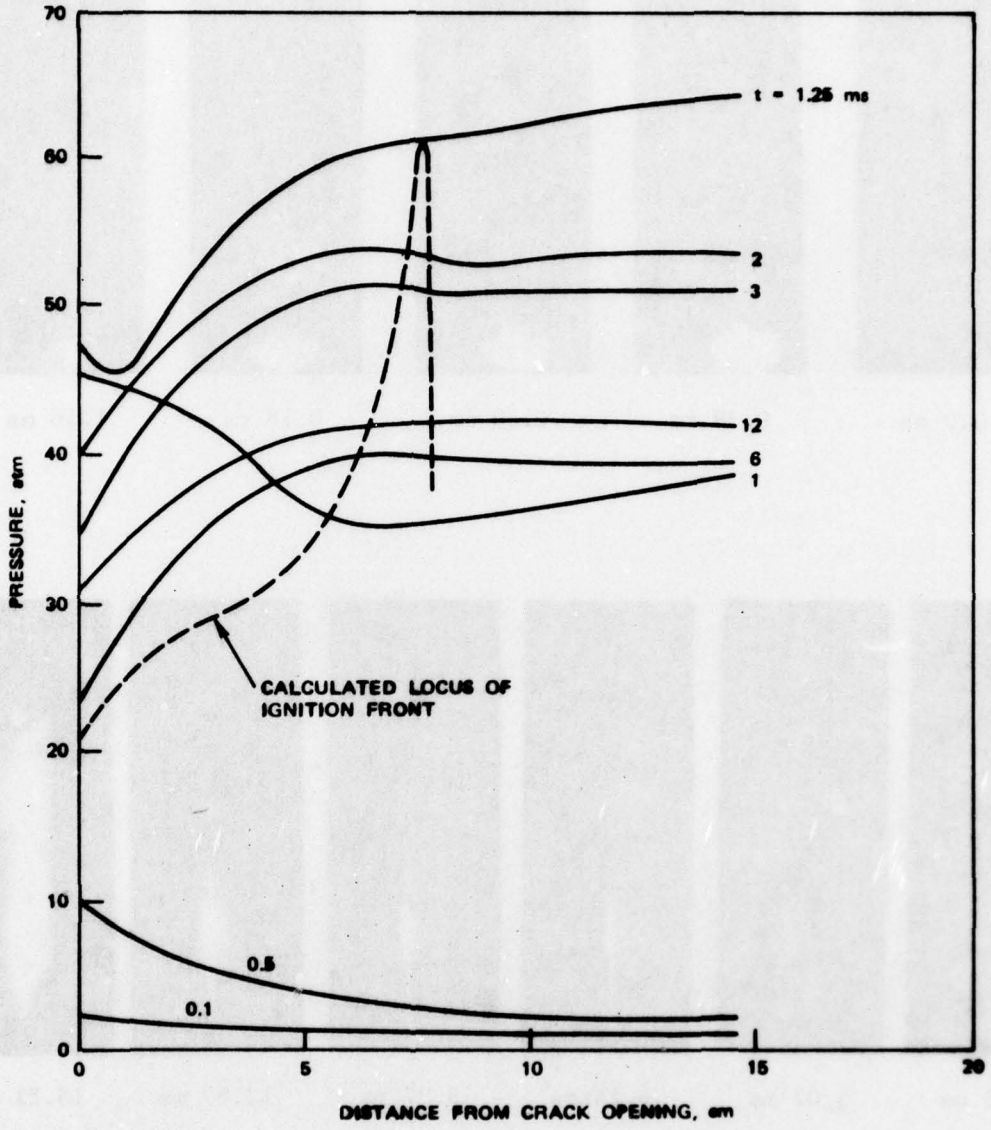

FIGURE 19. Calculated Pressure Distribution at Various Times (Simulation of DNC Test No. 21).

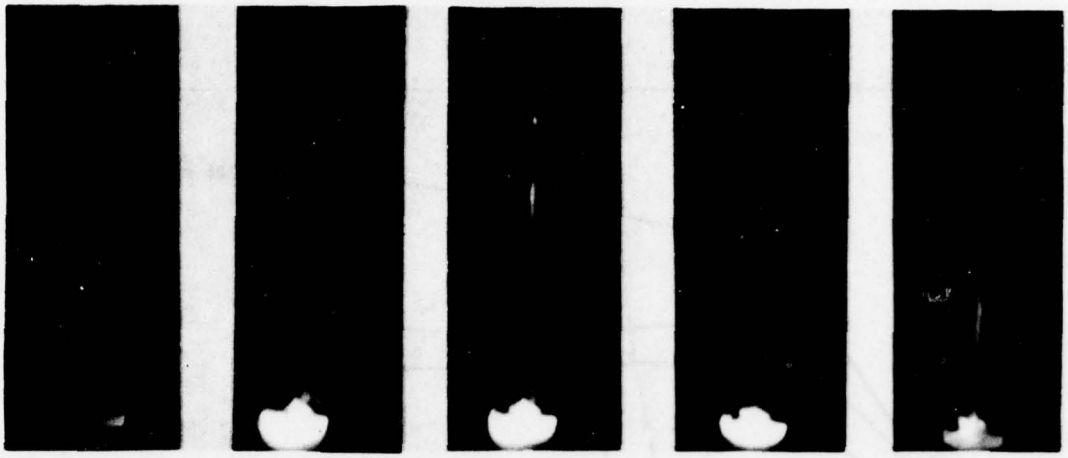

0.0 ms 0.39 ms 0.59 ms 0.78 ms 1.56 ms

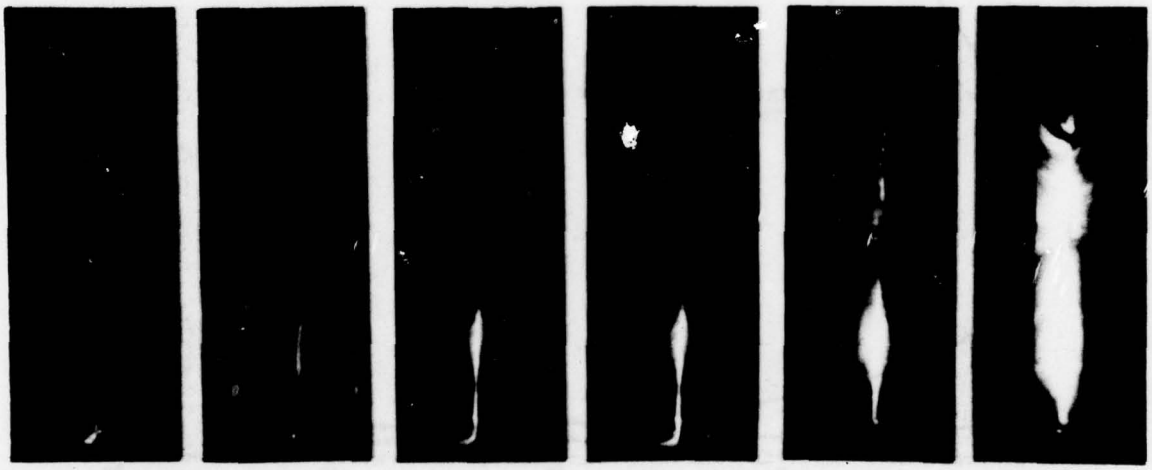

2.73 ms 5.07 ms 6.24 ms 8.97 ms 12.87 ms 15.21 ms

FIGURE 20. Motion Pictures of the Ignition and Combustion Phenomena in a Solid Propellant Crack of DNC Test No. 21.

TABLE 6. Physical Interpretation of the Film of DNC Test No. 21.

Picture No.	Time, ms	Observations and interpretations
1	0.0	Hot igniter gas enters the rectangular duct in the bottom of the main chamber
3	0.39	The hot igniter gas penetrates into the crack
4	0.59	High intensity gases appear at the tip of the crack
5	0.78	High intensity gases disappeared from the tip
9	1.56	The booster piece, attached to the left leg at the crack entrance, burns severely
15	2.73	High intensity light in the region near the crack opening
27	5.07	After a period of decrease in light intensity, the intensity increases again
32	6.24	The flame is not propagating
47	8.97	The flame still has not advanced further up the crack
67	12.87	The flame is not propagating up the crack
79	15.21	The entire crack is ignited

crack is very low; this is mainly due to the stagnation point condition at the crack tip. Another reason for the low velocity in this region is the lack of a favorable pressure gradient as the driving potential. The low flow velocity significantly reduces the convective heating of the propellant surface. Hence, a much longer time is required for the propellant surface near the crack tip to achieve a state of ignition. This delay is readily evident in both the calculated locus of ignition shown in Figure 19 and the high-speed film in Figure 20.

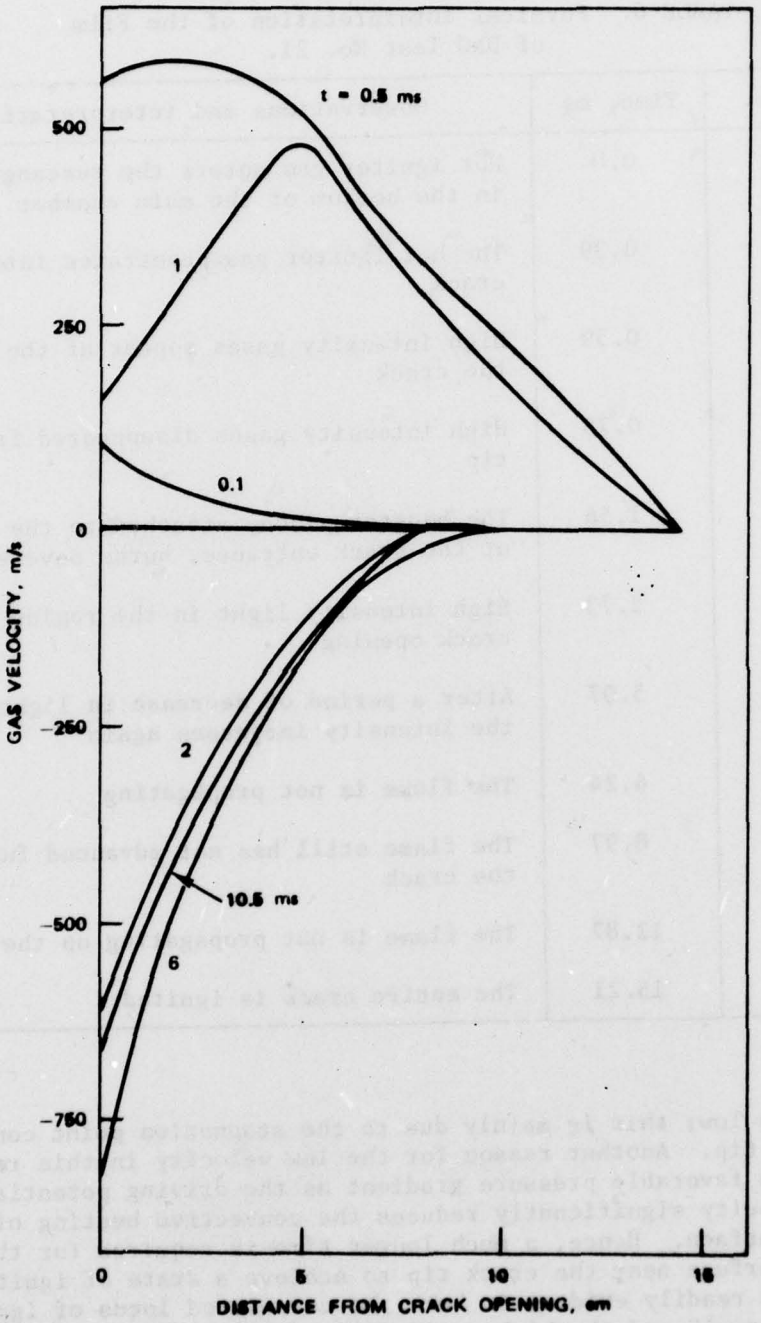

FIGURE 21. Calculated Velocity Distribution at Various Times (Simulation of DNC Test No. 21).

Figure 22 gives the calculated gas temperature distribution along the crack at various times. The temperature gradients at 0.1 and 0.5 ms are very pronounced near the opening of the crack indicating the penetration of hot gases into the propellant crack. Figure 22 shows that the gas temperature is lowest near the tip of the crack. The local gas temperature is low because no favorable pressure gradient exists to cause the hot gases to flow into the stagnation region near the closed end of the crack.

Figure 23 describes the propellant surface temperature distribution at various times. The curve for 0.1 ms shows that the propellant surface near the crack entrance is slightly above the ambient temperature of 298°K due to convective heating of the propellant surface. At 0.5 ms, the propellant surface temperature has a sharp gradient near the crack entrance caused by strong convective heating. The surface temperature increases continuously until the state of ignition is reached. In the model, the surface temperature is kept constant at 920°K after the propellant is ignited. Therefore, the curves for the times of 1 and 6 ms have flat portions near the entrance of the crack where the propellant is burning. The propellant surface temperature near the closed-end or tip of the crack remains low since convective heating of the propellant surface is significantly lower in this region than the crack entrance region.

Figure 24 shows the calculated growth of the crack gap due to combustion. Since there is no ignition at 0.1 ms, the initial crack gap profile is the same as the curve labeled t = 0.1 ms. For the time period shown, most of the contour change occurs near the open end of the crack. The amount of surface regression is the highest at the crack opening since the propellant has been burning for a longer period of time; the erosive burning effect also contributes to the total regression in this region.

PROBLEM AREAS IN THE STUDY OF PROPELLANT CRACK COMBUSTION

In recent years, a significant amount of work has been conducted in the investigation of crack combustion in the USA and also in other countries such as the USSR, Japan, and England. However, the convective burning in solid propellant cracks is not yet fully understood and many problems have not been completely solved. It is beneficial, in the authors' opinion, to list some of the unsolved problems here so that the technological gaps in this area are identified. It should be noted that some of the problems listed are the immediate subject areas that are being investigated at the Pennsylvania State University but other problems may take years before adequate answers are obtained. Hopefully the following list of questions may stimulate further interest among the researchers in finding solutions to these problems.

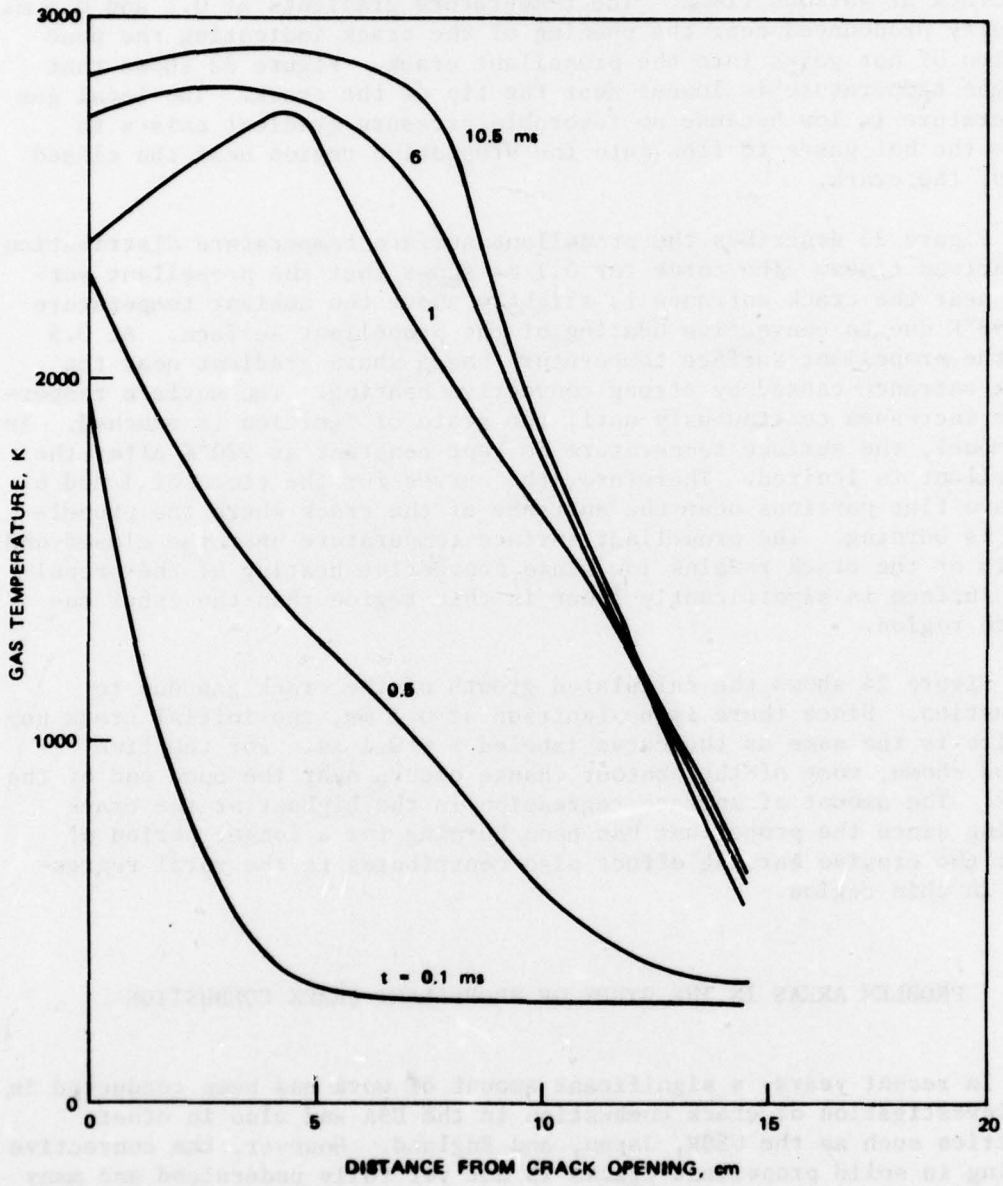

FIGURE 22. Calculated Gas Temperature Distribution for Various Times (Simulation of DNC Test No. 21).

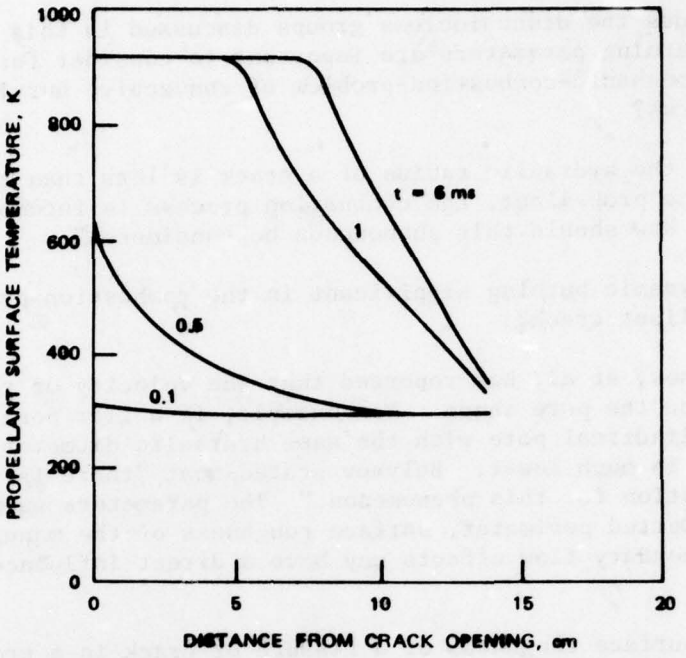

FIGURE 23. Calculated Propellant Surface Temperature Distribution at Various Times (Simulation of DNC Test No. 21).

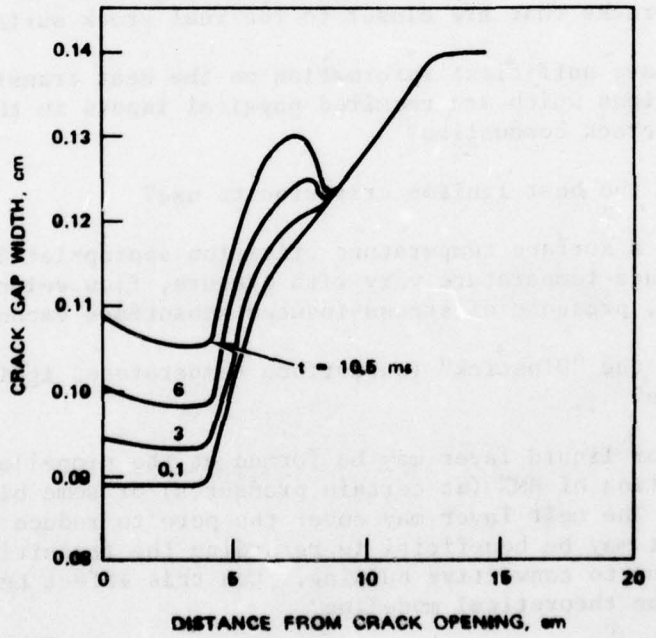

FIGURE 24. Calculated Growth of Crack Gap Due to Combustion (Simulation of DNC Test No. 21).

1. Besides the dimensionless groups discussed in this report, what other governing parameters are important to consider for the coupled solid-mechanic-combustion problem of convective burning in solid propellant cracks?

2. When the hydraulic radius of a crack is less than the flame thickness of the propellant, the combustion process is incomplete in the local region. How should this phenomenon be considered?

3. Is dynamic burning significant in the combustion processes inside a propellant crack?

4. Belyaev, et al. has reported that the velocity of the flame front depends on the pore shape. For example, if a flat pore is replaced by a cylindrical pore with the same hydraulic diameter, the flame spreading rate is much lower. Belyaev stated that "there is no satisfactory explanation for this phenomenon." The parameters such as ratio of burning-to-wetted perimeter, surface roughness of the manufactured cracks, and secondary flow effects may have a direct influence in this phenomenon.

5. The surface roughness of a fissure or crack in a propellant grain can differ appreciably from that of a manufactured crack. The projections of AP crystals or binder in a rough crack would be easier to ignite and would result in a faster flame spreading rate. How should one manufacture cracks that are closer to the real crack surface?

6. Do we have sufficient information on the heat transfer and friction correlations which are required physical inputs in the theoretical modeling of crack combustion?

7. What is the best igniton criterion to use?

   a. Is a surface temperature criterion appropriate? How does the critical surface temperature vary with presure, flow velocity, surface roughness, presence of stress-induced subsurface vacuoles, etc.?

   b. Is the "Dipstick" (subsurface temperature) ignition criterion suitable?

8. A melt or liquid layer may be formed at the propellant surface during the combustion of HMX (at certain pressures) or some binders such as polyurethane. The melt layer may cover the pore to reduce the pore size. This effect may be beneficial in retarding the transition from normal deflagration to convective burning. Can this effect be adequately described in the theoretical modeling?

9. According to Boggs, et al., cracks can develop during the burning of HMX crystals due to steep subsurface thermal gradients. Unlike the melt layer effect described above, these micropores should contribute to the transition from normal deflagration to convective burning. How should these micropores be treated in the theoretical modeling?

10. For metallized propellants, what is the role of the metal particles in the ignition and combustion processes inside cracks--especially, when the melted particle diameter is of the same order as the hydraulic diameter of the crack?

11. Closure of a burning propellant crack due to stress wave interactions may cause extinction. What degree of closure is required to cause extinction?

12. The accelerated convective burning inside propellant cracks can cause the formation of shock-like fronts in the gas phase. What is the mechanism of transition from these pressure fronts to a shock or detonation wave in porous propellants? What role do stress-induced vacuoles play in the transition from convective burning to low velocity detonation (LVD) or detonation (adiabatic compression, etc.)?

13. What is the functional form of the propellant stress-strain equation? Is a nonlinear viscoelastic model, $\sigma = \sigma(t,\varepsilon,\dot{\varepsilon},T,P, \text{etc.})$, absolutely essential? Are there sufficient data available to characterize the propellant constitutive equation?

14. In the thermal penetration layer of burning propellants, are thermal stresses significant? More importantly, is the propellant thermorheologically simple for temperatures approaching 800-1000°K? Answers to these questions are necessary in selecting the number and size of finite elements in the stress analysis.

SUMMARY OF PROGRESS AND CONCLUSIONS

1. The governing equations for describing the heat transfer and gas dynamic processes in solid propellant cracks have been nondimensionalized. A set of governing dimensionless parameters has been obtained to help future data correlation and analysis.

2. A number of modifications have been made in the crack combustion program. The major ones are given in the following:

a. In order to obtain more information about the in-depth thermal profile of the propellant, the one-dimensional transient heat-conduction equation was solved by an explicit, variable-mesh finite-difference method. The propellant surface temperature can be determined either by the finite difference solution of the partial differential equation for heat conduction or by the Goodman integral method.[7] The "Dipstick" ignition criterion, postulated by Price* has been incorporated in the crack combustion program.

b. The boundary condition at the entrance of the crack has been improved. The program can now more accurately describe the influence of rapidly varying rocket chamber pressurizations on the subsonic and sonic inflow of gases.

c. The restart feature of the crack combustion code has been improved to stop the calculation at any desired time to examine the solution, thus, saving both time and money. (The most up-to-date version of the crack combustion program was sent to NWC in February 1978.)

3. To facilitate the photographic recording of the transient flame spreading event, a reproducible and reliable solid propellant igniter system has been designed, fabricated, and tested to replace the previously developed gaseous igniter. The purpose of this replacement is to reduce the time interval between the onset of the igniter and the first ignition inside the crack.

4. To simulate chamber pressurization during the ignition transient of a rocket motor or the sudden pressurization for an initially submerged crack in a solid propellant, the pressurization rate of the crack combustion chamber is controlled by varying the igniter charge weight, the flow areas of the inlet and exit nozzles in the combsution chamber.

5. Numerous test firings have been conducted in the crack combustion chamber to determine the influence of the solid propellant igniter on the flame spread and pressurization in single-pore propellant samples. The previously reported debond problem[3] at the interface between the propellant sample and the brass mold has been solved.

6. A procedure has recently been developed to fabricate propellant samples from propellant slabs to form slit-type cracks. This in-house fabrication procedure has the following advantages: (1) economy, (2) well controlled crack geometry, (3) wide range of crack length to gap width ratios, and (4) the flexibility of viewing the flame spreading from different orientations.

---

*Private communication with Channon F. Price, Naval Weapons Center, April 1977.

7. The crack combustion chamber has been modified and various components have been fabricated to accommodate both the NWC cast specimens and the PSU fabricated propellant cracks.

8. A literature survey on crack fracture and deformation has been conducted. From this review, a modified version of NONSAP (NFAP) has been selected to couple with the crack combustion code and the NFAP code has been obtained and loaded on the Pennsylvania State University computer.

9. The comparison of the theoretical results with experimental pressure-time traces showed good qualitative agreement. Although the quantitative comparison showed a reasonable match, some differences were noted. In order to improve the predictive capabilities of the theoretical model, the following physical phenomena must be considered:

a. incorporation of solid mechanics of the propellant into the crack combustion model;

b. possible ignition of propellant in the crack tip region caused by a mechanism other than convective heating of the propellant surface; and

c. dynamic burning behavior of the propellant under rapid transient pressure excursions.

Appendix A

CHECK LIST OF CRACK COMBUSTION TEST PROCEDURE

1. Focus the camera and set the f-stop at the desired position.

2. Check that the START/STOP switch on the camera speed controller is in the STOP position.

3. Make sure that test cell power, ignition, and solenoid de-activation switches are all in OFF (down) position prior to film loading in camera.

4. Record the framing rate (PPS) from the setting on speed controller and the f-stop from camera.

5. Set the LED driver switch to the ON position. Set the pulse rate (pulses/s) of the LED maker and record the rate.

6. Check to ensure that the camera and LED driver electrical plugs are securely inserted in power receptacles.

7. Mount the igniter system onto the crack combustion chamber. Leave the safety plug in the solenoid armature.

8. Establish flow of water to transducers and check for leaks.

9. Check firing relay box to ensure that

   a. Common-time leads are connected to both the camera and tape recorder inputs
   b. 110 VAC solenoid lead is connected to relay from power source
   c. 12 VDC connected to electromagnet input

10. Activate ONLY test cell power switch. (Must be on for a minimum of 20 seconds prior to firing with the camera speed controller.)

11. Perform a final check of switches and leads

    a. Transducers leads, charge amplifiers, and tape inputs conform to that previously checked on DATA SHEET
    b. Charge amplifiers in: (1) CHARGE mode, (2) GROUNDED position

c. Both toggle switches on calibration panel are in OFF (up) position and rotary switch is in a null position.

12. Turn ON test cell exhaust fan.

13. Perform the following actions in the test cell:

a. Check that the LED driver power light is ON
b. Ensure that the common-time trip indicator on LED driver is not lit
c. Connect lead from relay box to solenoid armature
d. Turn ON camera lights
e. ARM THE SYSTEM by removing the solenoid safety plug
f. Close the test cell door

14. Firing Officer then:

a. Starts tape drive in RECORD mode
b. Says: "DNC Test No. ___," the date, "Unground Charge Amplifiers," the "Fire" (while simultaneously activating the IGNITION switch)
c. Immediately after percussion element discharges, turn ON (flip up) the solenoid de-activation switch
d. NEVER turn off test cell power or ignition switches while the combustion event is occurring . Allow ample time for the entire film to transport to take-up reel.
e. STOP tape immediately after the firing is completed and then GROUND charge amplifier.
f. Turn OFF: camera lights; test cell power, ignition, and solenoid de-activation switches; and then cooling water to transducers if any leaks appear in water lines.

15. Put calibration signals on magnetic tape.

a. Start tape drive in RECORD mode and say "Calibration"
b. Simulate a pressure in the charge amplifiers by applying a negative DC voltage to the charge amplifier calibration inputs, then switch charge amplifiers to both CAL mode and OPERATE position and then switch second toggle switch on calibration panel down for say only 3-5 seconds. Finally, GROUND charge amplifiers and turn off the tape recorder.

16. Use a black hood when removing film from the camera and specify all information on the film box.

17. Put all remarks on DATA SHEET however trivial they may be (i.e., did all the crack burn, etc.). Use a Kodak Instamatic or press camera to record all interesting disassembly views.

Appendix B

DATA SHEET FOR DN CRACK PROJECT

COMBUSTION TEST No. _____

DATE _____

TEMPERATURE: T_{room} _____ °F T_{soil} _____ °F

CRACK GEOMETRY:

TYPE _____

LENGTH _____

ENTRANCE WIDTH _____

TIP WIDTH _____

IGNITER:

PRIMER _____

BOOSTER _____

MASS/LENGTH _____

IGNITER PASTE _____

CAMERA:

LENS & f/STOP _____

FRAMING RATE _____ FRAMES/s

TIMER MARKER _____ PULSES/s

REMOTE FIRING AT _____ FT OF FILM

PICTURES PER FRAME _____

FILM:

ASA No. _____ , TYPE _____

BLACK & WHITE _____ , COLOR _____

NOZZLES:

PERFORATED _____

EXIT _____

DATA ACQUISITION:

TAPE No. _____ , TAPE LOCATION _____ TO _____ , TAPE SPEED _____ in./s

	X DIST.	GAGE TYPE AND SERIAL No.	TAPE CHANNEL	TRANSDUCER SENSITIVITY (KISTLER)	RANGE MULTIPLIER	TIME CONSTANT	K psi/V	CALIB. VOLTS
G–1								
G–2								
G–3								
G–4								
G–5								
COMMON TIME								
VOICE								

PARTICIPANTS:

REMARKS: BURSTING DIAPHRAGM _____ , P_{max} = _____ , No. OF TIMES USED _____

NOMENCLATURE

A_b	Burning surface area
An	Andreev number
A_p	Cross-sectional area of the crack, cm^2
A_{px}	The spatial change of cross-sectional area of crack with respect to the axial distance, cm
A_w	Area of inert wall
a	Pre-exponential factor in the nonerosive burning rate law, ap^n $(cm/s)(cm^2/g_f)^n$
B_x	Body force, g_f/g
b	Co-volume, cm^3/g
c	Speed of sound, cm/s; when with subscript, specific heat, cal/g-°K
c_f	Friction coefficient, $2g\tau_w/\rho u^2$
c_p	Specific heat at constant pressure, cal/g-°K
D_H	Hydraulic diameter of the crack, cm
E	Total stored energy (internal and kinetic), cal/g
g	Acceleration of gravity, conversion factor, $g\text{-}cm/g_f\text{-}s^2$
H	Depth of the gap in flow visualization tests, cm
$\bar{h}_c$	Local convective heat transfer coefficient, $cal/cm^2\text{-}s\text{-}°K$
$\bar{h}_{cp}$	Local convective heat transfer coefficient over the propellant surface, $cal/cm^2\text{-}s\text{-}°K$
$\bar{h}_{cw}$	Local convective heat transfer coefficient over non-propellant pore wall, $cal/cm^2\text{-}s\text{-}°K$
h_f	Enthalpy of combustion gas at adiabatic flame temperacure, cal/g
J	Mechanical equivalent of heat, $g_f\text{-}cm/cal$
K_e	Erosive burning constant, $cm^3\text{-}°K/cal$
L	Length of the crack, cm
M_w	Molecular weight, g_f/g-mole
n	Pressure exponent in the nonerosive burning rate law
P	Static pressure, g_f/cm^2
Pr	Prandtl number
p_b	Burning perimeter, cm
p_w	wetted perimeter of the port, cm
R	Specific gas constant for the combustion gases, $g_f\text{-}cm/g\text{-}°K$
Re	Reynolds number
r_b	Burning rate of the solid propellant, including the erosive burning contribution, cm/s
St*	Stanton number
T	Temperature (without subscript, static gas temperature), °K
T_{af}	Average film gas temperature $(T + T_{ps})/2$, °K
T_f	Adiab
T_{pi}	Initi
T_{ps}	Prope
T_{ws}	Nonpr
t	Time,
u	Gas v
V_{gf}	The v
V_k	The c
x	Axial
x_L	Posit
x_p	Axial
y	Perpe sol
α	Therm
β	Erosi
γ	Ratio
δ	Gap w
ε	A sma
ε_s	Surfa
θ_w	Angle of
λ	Therm
μ	Gas v
ρ	Densi
τ_w	Shear
τ_{xx}	Norma
~	Dimens
*	Refere

Subscripts

c	Rocket
cri	Critic
fp	Flame
fs	Flame
i	Initia
ign	Igniti
pr	Propel
th	Therma

crack with respect

ing rate law,

pecific heat, cal/g-°K

cal/g
g-cm/g_f-s^2
, cm
cal/cm^2-s-°K
ver the propellant
ver non-propellant
e temperature, cal/g

rate law

es, g_f-cm/g-°K
ing the erosive
emperature), °K

T_f Adiabatic flame temperature of the solid propellant, °K
T_{pi} Initial propellant temperature, °K
T_{ps} Propellant surface temperature, °K
T_{ws} Nonpropellant wall surface temperature, °K
t Time, s
u Gas velocity, cm/s
V_{gf} The velocity of propellant gas at the burning surface, cm/s
V_k The coefficient in viscosity-temperature relation
x Axial distance from propellant crack opening, cm
x_L Position at the end of crack, cm
x_p Axial distance along the crack at which propellant begins, cm
y Perpendicular distance from the propellant surface into the solid, cm
α Thermal diffusivity, cm^2/s
β Erosive burning exponent
γ Ratio of specific heats
δ Gap width of the crack, cm
ε A small number of °K
ε_s Surface roughness, cm
θ_w Angle measured, in a counterclockwise direction, at the lower side of the propellant, degree
λ Thermal conductivity, cal/cm-s-°K
μ Gas viscosity, g/cm-s (poise)
ρ Density (without subscript, gas density), g/cm^3
τ_w Shear stress on the port wall, g_f/cm^2
τ_{xx} Normal viscous stress, g_f/cm^2
~ Dimensionless parameters
* Reference parameters

Subscripts

c Rocket chamber
cri Critical condition for surface ablation
fp Flame propagation
fs Flame stand-off
i Initial value
ign Ignition condition
pr Propellant
th Thermal wave thickness

2

INITIAL DISTRIBUTION

1 Director of Navy Laboratories
8 Naval Air Systems Command
  AIR-30212 (2)
  AIR-330 (1)
  AIR-330B, Robert H. Heitkotter (1)
  AIR-330D (1)
  AIR-536 (1)
  AIR-954 (2)
4 Chief of Naval Operations
3 Chief of Naval Material
  MAT-03 (1)
  MAT-03PB (1)
  MAT-08E17, Dr. June Amlie (1)
7 Naval Sea Systems Command
  SEA-03 (1)
  SEA-033 (1)
  SEA-0331, Murrin (1)
  SEA-0331B, Cassel (1)
  SEA-0332 (1)
  SEA-09G32 (2)
9 Chief of Naval Research, Arlington
  ONR-100 (1)
  ONR-102 (1)
  ONR-401 (1)
  ONR-420 (1)
  ONR-472 (1)
  ONR-473
    Richard Miller (1)
    James R. Patton, Jr. (1)
  ONR-474, Dr. N. Basdekas (1)
3 Naval Ordnance Station, Indian Head
  Code 525, Peter Stang (1)
  Code 5251K, Fred Robbins (1)
  Technical Library (1)
3 Naval Postgraduate School, Monterey
  Code 57, Fuhs (1)
  Code 57NT, Netzer (1)
  Technical Library (1)
6 Naval Research Laboratory
  Code 2021 (1)
  Code 5570, Optical Sciences Division, Dr. J. Schnur (1)

Code 6120, Dr. W. Moniz (1)
Code 6130, Chemistry Division (1)
Dr. W. D. Bascom (1)
Technical Library (1)
1 Naval Surface Weapons Center, Dahlgren Laboratory, Dahlgren
(D. R. McClure)
9 Naval Surface Weapons Center, White Oak
WR-10
Julius W. Enig (1)
Donna Price (1)
WR-13
Dr. R. Bernecker (1)
C. Coffey (1)
Nathaniel L. Coleburn (1)
Dr. S. J. Jacobs (1)
Kibong Kim (1)
WR-20, William E. McQuistion (1)
G. B. Wilmot (1)
1 Naval Underwater Systems Center, Newport (Code 5B331, Robert S. Lazar)
1 Naval Weapons Evaluation Facility, Kirtland Air Force Base (Code 401)
3 Navy Strategic Systems Project Office
NSP-2731
Roy Kinert (1)
L. Throckmorton (1)
Dr. J. F. Kincaid (1)
1 Office of Naval Research, Boston (Dr. Larry Peebles)
1 Office of Naval Research Chicago (Dr. Jerry J. Smith)
1 Army Armament Materiel Readiness Command, Rock Island (DRSAS-LEM,
Richard Zastrow)
4 Army Armament Research and Development Command, Dover
ASD/LCWSL, Dr. J. Hershkowitz (1)
DRDAR-LCE, Dr. R. F. Walker (1)
DRDAR-SCA-PE, L. Stiefel (1)
LCWSL, C. Lenchitz (1)
1 Army Materiel Development and Readiness Command (DRCDE-DW, Stephen R.
Matos)
1 Army Missile Research and Development Command, Redstone Arsenal
(DRDMI-RK, Dr. R. G. Rhoades)
1 Army Armament Research and Development Center (SMUPA-TS-TS, J. Picard)
6 Army Ballistic Research Laboratories, Aberdeen Proving Ground
DRDAR-BLP
Austin W. Barrows (1)
Ingo W. May (1)
L. A. Watermeier (1)
DRDAR-BLT, Dr. Robert Frey (1)
DRDAR-TSB-S (STINFO) (1)
Dr. D. E. Kooker (1)

1 Rock Island Arsenal (Edward Haug)
1 Air Force Armament Laboratory, Eglin Air Force Base (DLDL, Otto K. Heiney)
3 Air Force Rocket Propulsion Laboratory, Edwards Air Force Base
  DYSC, Wilbur C. Andrepont (1)
  MKP, R. L. Geisler (1)
  Daweel George (1)
2 Air Force Office of Scientific Research
  Joseph F. Masi (1)
  Bernard T. Wolfson (1)
12 Defense Documentation Center
1 National Aeronautics and Space Administration (Code RP, Frank W. Stephenson, Jr.)
3 George C. Marshall Space Flight Center
  EP-25, Dr. Ben Shackelford (1)
  SE-ASTN-PEA, John Q. Miller (1)
  Richard J. Richmond (1)
1 Lewis Research Center (Richard J. Priem)
1 Lyndon B. Johnson Space Center (EP, Joseph G. Thibodaux)
2 Aerojet Solid Propulsion Company, Sacramento, CA (Via AFPRO)
  Dept 4350, M. Ditore (1)
  Dr. Adolph E. Oberth (1)
1 Aeronautical Research Associates of Princeton, Inc., Princeton, NJ (E. S. Fishburne)
1 Aerospace Corporation, Los Angeles, CA (Ellis M. Landsbaum)
1 Allegany Ballistics Laboratory, Cumberland, MD (Roy R. Miller)
1 Analy Syn Laboratories, Paoli, PA (Dr. V. Keenan)
1 Atlantic Research Corporation, Alexandria, VA (Merrill K. King)
1 Battelle Memorial Institute, Columbus, OH (Abbott A. Putman)
1 Brigham Young University, Provo, UT (673/W1dB, L. Douglas Smoot)
1 California Institute of Technology, Pasadena, CA (Prof. Wolfgang Knauss)
1 California State University Sacramento, Sacramento, CA (School of Engineering, Frederick H. Reardon)
1 Calspan Corporation, Buffalo, NY (Edward B. Fisher)
1 Carnegie-Mellon Institute, Pittsburgh, PA (Dept of Mathematics, Dr. M. Gurtin)
1 Chemical Propulsion Information Agency, Applied Physics Laboratory, Laurel, MD (Thomas W. Christian)
4 Georgia Institute of Technology, Atlanta, GA
  Ben T. Zinn (1)
  Edward W. Price (1)
  Dr. Robert K. Sigman (1)
  Warren C. Strahle (1)
1 General Applied Science Laboratory, Westbury Long Island, NY (John Erdos)
1 General Dynamics Corporation, Pomona Division, Pomona, CA (Paul L. Boettcher)
1 Gough Associates, Inc., Portsmouth, NH (Dr. Paul Gough)

6 Hercules Incorporated, Bacchus, Works, Magna, UT
  Dr. McKay Anderson (1)
  Dr. B. Hopkins (1)
  Ken McCarty (1)
  Dr. D. Pilcher (1)
  Ronald L. Simmons (1)
  Dr. J. Thatcher (1)
1 Hercules Incorporated, McGregor, TX (William G. Haymes)
1 IIT Research Institute, Chicago, IL (Dr. Tom Eichler)
1 Institute for Defense Analyses, Arlington, VA (R. C. Oliver)
4 Jet Propulsion Laboratory, Pasadena, CA
  N. Cohen (1)
  Fred E. C. Culick (1)
  Leon D. Strand (2)
4 Lockheed Missiles and Space Company, Sunnyvale, CA
  J. Linsk (1)
  H. Marshall (1)
  R. Martinson (1)
  Dr. Vern Orr (1)
5 Los Alamos Scientific Laboratory, Los Alamos, NM
  B. Craig, Group MS-960 (1)
  Dr. C. Forest, T14 (1)
  Dr. Randy Peeters, MS-931WX-3 (1)
  Dr. Louis C. Smith (1)
  J. D. Wackerle, WX-7 (950) (1)
1 Materials Sciences Corporation, Blue Bell, PA (Dr. Z. Hashin)
1 Northwestern University, Evanston, IL (Dept of Civil Engineering, Dr. Jan Achenbach)
25 Pennsylvania State University, University Park, PA (Prof. K. K. Kuo)
3 Princeton University, Forrestal Campus Library, Princeton, NJ
  Leonard H. Caveny (1)
  W. Sirignano (1)
  Dr. Martin Summerfield, Dept of Aerospace and Mechanical Engineering (1)
1 Purdue University, West Lafayette, IN (School of Mechanical Engineering, John R. Osborn)
2 Rockwell International Corporation, Canoga Park, CA
  BA08, Joseph E. Flanagan (1)
  Dept 589-197-SS11, Carl L. Oberg (1)
1 Rohm and Haas Company, Huntsville, AL (Dr. Henry M. Shuey)
1 SRI International, Menlo Park, CA (Dr. D. R. Curran)
1 Science Applications, Inc., Woodland Hills, CA (R. B. Edelman/Suite 423)
1 Southwest Research Institute, San Antonio, TX (Fire Research Section, William H. McLain)
1 TRW Systems, Inc., Redondo Beach, CA (A. C. Ellings)

2 Texas A&M University, College Station, TX
Department of Civil Engineering
Dr. S. C. Britton (1)
Prof. R. A. Schapery (1)
1 The University of Akron, Akron, OH (Institute of Polymer Science, Dr. A. N. Gent)
1 Thiokol Corporation, Huntsville Division, Huntsville, AL (David A. Flanigan)
2 Thiokol Corporation, Wasatch Division, Brigham City, UT
John A. Peterson (1)
Mark Weiner (1)
1 United Technologies Corporation, East Hartford, CT (R. H. W. Waesche)
3 United Technologies Corporation, Sunnyvale, CA
Chemical Systems Division
Robert S. Brown (1)
Eugene C. Francis (1)
Dr. B. L. Iwanciow (1)
1 Universal Propulsion Company, Riverside, CA (H. J. McSpadden)
4 University of California, Lawrence Radiation Laboratory, Livermore, CA
H. Cheung (1)
E. James (1)
E. Lee (1)
Dr. P. Urtiew (1)
1 University of California, San Diego, LaJolla, CA (AMES Dept, Forman A. Williams)
1 Unviersity of Illinois, Urbana, IL (AAE Dept, Herman Krier)
1 University of Southern California, Los Angeles, CA (Mechanical Engineering Dept/OHE200, M. Gerstein)
2 University of Texas, Austin, TX
Center for Statistical Mechanics and Thermodynamics, Dr. J. S. Turner (1)
Dept of Aerospace Engineering and Engineering Mechanics, Dr. Eric Becker (1)
4 University of Utah, Salt Lake City, UT
Dept of Chemical Engineering, Alva D. Baer (1)
G. A. Flandro (1)
Prof. Stephen R. Swanson (1)
1 Washington State University, Pullman, WA (Department of Physics, Dr. G. E. Duvall)
2 Whittaker Corporation, Bermite Division, Saugus, CA
L. Bloom (1)
L. LoFiego (1)